


## TRANSLATIONAL SCIENCE

## Pathogenic neuropsychiatric effect of stress-induced microglial interleukin 12/23 axis in systemic lupus erythematosus

Nobuya Abe ,<sup>1,2</sup> Masato Tarumi,<sup>1,2</sup> Yuichiro Fujieda ,<sup>2</sup> Nobuhiko Takahashi,<sup>1</sup> Kohei Karino,<sup>2</sup> Mona Uchida,<sup>1</sup> Michihito Kono ,<sup>2</sup> Yuki Tanaka,<sup>1,3</sup> Rie Hasebe,<sup>4,5</sup> Masaru Kato ,<sup>2</sup> Olga Amengual,<sup>2</sup> Yoshiyuki Arinuma ,<sup>6</sup> Kenji Oku,<sup>2,6</sup> Wakiro Sato,<sup>7</sup> Khin Khin Tha,<sup>8,9</sup> Miwako Yamasaki,<sup>10</sup> Masahiko Watanabe,<sup>10</sup> Tatsuya Atsumi,<sup>2</sup> Masaaki Murakami <sup>1,3,5</sup>

Handling editor Josef S Smolen

► Additional supplemental material is published online only. To view, please visit the journal online (<http://dx.doi.org/10.1136/ard-2022-222566>).

For numbered affiliations see end of article.

**Correspondence to**

Professor Masaaki Murakami, Division of Molecular Psychoimmunology, Institute for Genetic Medicine, Graduate School of Medicine, Hokkaido University, Sapporo, Japan; [murakami@igm.hokudai.ac.jp](mailto:murakami@igm.hokudai.ac.jp) and Professor Tatsuya Atsumi, Department of Rheumatology, Endocrinology and Nephrology, Faculty of Medicine, Hokkaido University, Sapporo, Japan; [at3tat@med.hokudai.ac.jp](mailto:at3tat@med.hokudai.ac.jp)

Received 29 March 2022  
Accepted 14 June 2022



© Author(s) (or their employer(s)) 2022. No commercial re-use. See rights and permissions. Published by BMJ.

**To cite:** Abe N, Tarumi M, Fujieda Y, et al. *Ann Rheum Dis* Epub ahead of print: [please include Day Month Year]. doi:10.1136/annrheumdis-2022-222566

**ABSTRACT**

**Objectives** The central nervous system disorder in systemic lupus erythematosus (SLE), called neuropsychiatric lupus (NPSLE), is one of the most severe phenotypes with various clinical symptoms, including mood disorder, psychosis and delirium as diffuse neuropsychological manifestations (dNPSLE). Although stress is one of the aggravating factors for neuropsychiatric symptoms, its role in the pathogenesis of dNPSLE remains to be elucidated. We aimed to investigate stress effects on the neuropsychiatric pathophysiology in SLE using lupus-prone mice and patients' data.

**Methods** Sleep disturbance stress (SDS) for 2 weeks was placed on 6–8-week-old female MRL/lpr and control mice. Behavioural phenotyping, histopathological analyses and gene and protein expression analyses were performed to assess SDS-induced neuroimmunological alterations. We also evaluated cytokines of the cerebrospinal fluid and brain regional volumes in patients with dNPSLE and patients with non-dNPSLE.

**Results** SDS-subjected MRL/lpr mice exhibited less anxiety-like behaviour, whereas stressed control mice showed increased anxiety. Furthermore, stress strongly activated the medial prefrontal cortex (mPFC) in SDS-subjected MRL/lpr. A transcriptome analysis of the PFC revealed the upregulation of microglial activation-related genes, including *Il12b*. We confirmed that stress-induced microglial activation and the upregulation of interleukin (IL) 12/23p40 proteins and increased dendritic spines in the mPFC of stressed MRL/lpr mice. IL-12/23p40 neutralisation and tyrosine kinase 2 inhibition mitigated the stress-induced neuropsychiatric phenotypes of MRL/lpr mice. We also found a higher level of cerebrospinal fluid IL-12/23p40 and more atrophy in the mPFC of patients with dNPSLE than those with non-dNPSLE.

**Conclusions** The microglial IL-12/23 axis in the mPFC might be associated with the pathogenesis and a promising therapeutic target for dNPSLE.

**INTRODUCTION**

Systemic lupus erythematosus (SLE) is an autoimmune disease with a predilection for young women of childbearing age, leading to a profound

**WHAT IS ALREADY KNOWN ON THIS TOPIC**

- ⇒ Neuropsychiatric lupus with diffuse neuropsychological manifestations (dNPSLE) is attributed to a variety of factors, including vascular occlusions, blood–brain barrier impairment, cytokines, autoantibodies and direct neuronal cell damage.
- ⇒ Stress affects the activation status of central neurons and glial cells, probably leading to neuroinflammation.
- ⇒ Stress, particularly chronic stress, is involved in the development of autoimmune diseases, including lupus, and has adverse effects on the disease activity with neuropsychiatric symptoms.

**WHAT THIS STUDY ADDS**

- ⇒ Stress-subjected MRL/lpr mice showed disinhibited behaviour, microglial activation with IL-12/23p40 upregulation and neuronal activation in the medial prefrontal cortex (mPFC).
- ⇒ Anti-IL-12/23p40 neutralising antibody or tyrosine kinase 2 inhibitor ameliorated these stress-elicited neuropsychiatric phenotypes in MRL/lpr.
- ⇒ A higher level of IL-12/23p40 in the cerebrospinal fluid and more atrophic changes in the mPFC were observed in patients with dNPSLE than those with non-dNPSLE.

**HOW THIS STUDY MIGHT AFFECT RESEARCH, PRACTICE AND/OR POLICY**

- ⇒ An association of the stress-elicited IL-12/23 axis in the mPFC with the pathogenesis of disinhibited agitative behaviour in patients with dNPSLE was suggested.
- ⇒ Blockade of IL-12/23 signalling in the mPFC may be a novel therapeutic target for dNPSLE.

impact on their lives. Patients with SLE manifest multiple organ disorders such as skin rash, arthritis, nephritis, haematologic abnormality and inflammation in the central nervous system (CNS).<sup>1</sup> Among them, CNS diseases occur in up to 50% of patients

and demonstrate a wide range of symptoms, including headache, stroke, anxiety, depression, cognitive dysfunction, seizures, psychosis and acute confusional state (ACS). The CNS disorder, neuropsychiatric SLE (NPSLE), is one of the most severe manifestations and is further classified into diffuse neuropsychological syndrome (dNPSLE) and focal neurological syndrome (fNPSLE). Although a variety of factors, including vascular occlusions, blood-brain barrier impairment, cytokines, autoantibodies and direct neuronal cell damage, have been suggested for the development of dNPSLE,<sup>2,3</sup> its pathogenesis remains poorly understood. In addition, neuropsychiatric symptoms often occur independently of the systemic disease activity among patients with SLE, making it difficult to predict the development of dNPSLE.<sup>4</sup> Rheumatologists have been using glucocorticoids and pancytotoxic immunosuppressants for treatment, but there is no available therapeutic strategy that targets the disease-specific pathogenesis.<sup>1,5</sup>

Stress as emotional and physiological challenges can affect the neural activation status in the CNS. In the short term, it promotes allostasis for adaptation to the surrounding environment, but in the long term, it exhausts the body physically and mentally. It has been known that stress affects the functions of several physiological systems via the neuroendocrine pathway.<sup>6</sup> Stress also targets and remodels the CNS itself structurally and functionally, contributing to alterations in behavioural and physiological responses.<sup>7</sup> In animal models, stress induced by sleep deprivation atrophies hippocampal and cortical neurons, resulting in impaired retention and memory.<sup>7-9</sup> Also, sleep deprivation increases cytokines and oxidative stress markers in neurons.<sup>7</sup> We previously reported sleep disturbance stress (SDS) induced brain microinflammation in the presence of CNS-specific autoreactive CD4-positive T cells, exacerbating clinical symptoms of experimental autoimmune encephalomyelitis (EAE).<sup>10</sup> Thus, stress together with immune cells would be involved in the exacerbation of autoimmune diseases. Indeed, SDS is reported to impair metabolism and upregulate proinflammatory cytokine in humans.<sup>11,12</sup> Stress exposure also increases the risk of developing autoimmune diseases, including lupus, and has adverse effects on the disease activity with neuropsychiatric manifestations in SLE.<sup>13,14</sup> However, the molecular mechanisms of stress on the dNPSLE pathogenesis are still unknown. Therefore, we here investigated whether SDS promotes neuropsychiatric symptoms and the molecular pathogenesis using lupus-prone mice and its association with patients with dNPSLE.

## PATIENTS, MATERIALS AND METHODS

Detailed information about each experiment and statistical analysis is described in online supplemental patients, materials and methods.

### Study design

Briefly, we used lupus-prone mouse models with SDS load. In animal experiments, 6–8-week-old female mice were used for each experiment. Behavioural phenotyping, histopathological analyses, RNA sequencing (RNA-seq), flow cytometry and ELISA were performed to assess SDS-induced behavioural changes and neuroimmunological alterations. We retrospectively reviewed medical records of the patients with SLE whose serum and cerebrospinal fluid (CSF) were preserved at Hokkaido University and Kitasato University between 2006 and 2020. We also collected the clinical data of 71 consecutive patients who underwent brain MRI at Hokkaido University Hospital between 2019 and 2020. We evaluated serum and CSF cytokine levels using ELISA and

atrophic brain regions using voxel-based morphometry (VBM) in the patients.

### Statistical analysis

Experimental data using mice were analysed with an unpaired Student's t-test and two-way analysis of variance with Tukey-Kramer post-hoc multiple comparisons test or paired t-test for the unpaired or paired values of continuous variables, respectively. For the analyses of human sample data, we used the Mann-Whitney U test and Kruskal-Wallis test with post-hoc Steel-Dwass multiple comparison method for the values of continuous variables and  $\chi^2$  test for the proportions of categorical variables. To explore differentially expressed genes in the RNA-seq analysis, we used adjusted p values with false discovery rate correction by the Storey method for genes with an absolute fold change (FC) over 1.5 compared with control strains. A receiver operating characteristics analysis was performed to evaluate the diagnostic ability of the data for dNPSLE with the area under the curve (AUC). Neuroimaging data were analysed by analysis of covariance with age, sex, disease duration, total intracranial volume and white matter (WM) volume as confounding factors. In the linear correlation analysis, Pearson's product moment correlation coefficients were calculated. P values lower than 0.05 were considered statistically significant. We used JMP Pro V.14 (SAS Institute, USA) for all analyses. All statistical tests were two-sided, and all experiments were performed at least two times.

## RESULTS

### Sleep disturbance stress-induced abnormal behaviour in lupus-prone mice

We employed MRL/MpJmsSlc-*lpr/lpr* (MRL/*lpr*) female mice, which show SLE-like manifestations, including nephritis and CNS symptoms.<sup>15</sup> For the stress load, we used SDS loading cages, in which continuous stress to inhibit regular sleep is imposed on mice on a free rotation wheel for 2 weeks (figure 1A, online supplemental figure 1A). Mice housed in SDS cages showed more activity throughout the night and higher levels of serum corticosterone than those housed in a normal cage (online supplemental figure 1B-F). We then performed behavioural phenotyping of SDS-subjected MRL/*lpr* mice and of control MRL/MpJmsSlc-*+/+* (MRL/MpJ) mice. We employed an elevated plus maze test (EPM) and open field test (OF) to assess risk-taking agitation-like behaviours, which are often observed in patients with dNPSLE with ACS as vigilance and psychomotor overactivity.<sup>16</sup> In the EPM, SDS-subjected control mice tended to show more anxiety-like behaviour than mice without stress, which is commonly seen in chronic stress-exposed mice. In contrast, SDS-subjected MRL/*lpr* showed significantly less anxiety-like behaviour than control (figure 1B,C). There was a slight but significant difference in total travelling distance in the EPM between the SDS-subjected MRL/*lpr* and control mice (figure 1D). Consistently, SDS-subjected MRL/*lpr* mice showed less anxiety-like behaviour than SDS-free MRL/*lpr* mice without any decrease in general locomotor activity in the OF (figure 1E-G). To exclude the possibility that systemic inflammation makes SDS-subjected mice disinhibited on the behaviour, we evaluated the SDS effect in NOD/ShiJcl, which is a mouse model of chronic inflammatory autoimmune disease like Sjögren's syndrome (SS). In contrast to SDS-subjected MRL/*lpr*, SDS-receiving NOD/ShiJcl demonstrated similar behaviour to SDS-free mice in the EPM (online supplemental figure 1G,H). Thus, stress had disinhibitory effects on the behaviours of MRL/*lpr* mice.

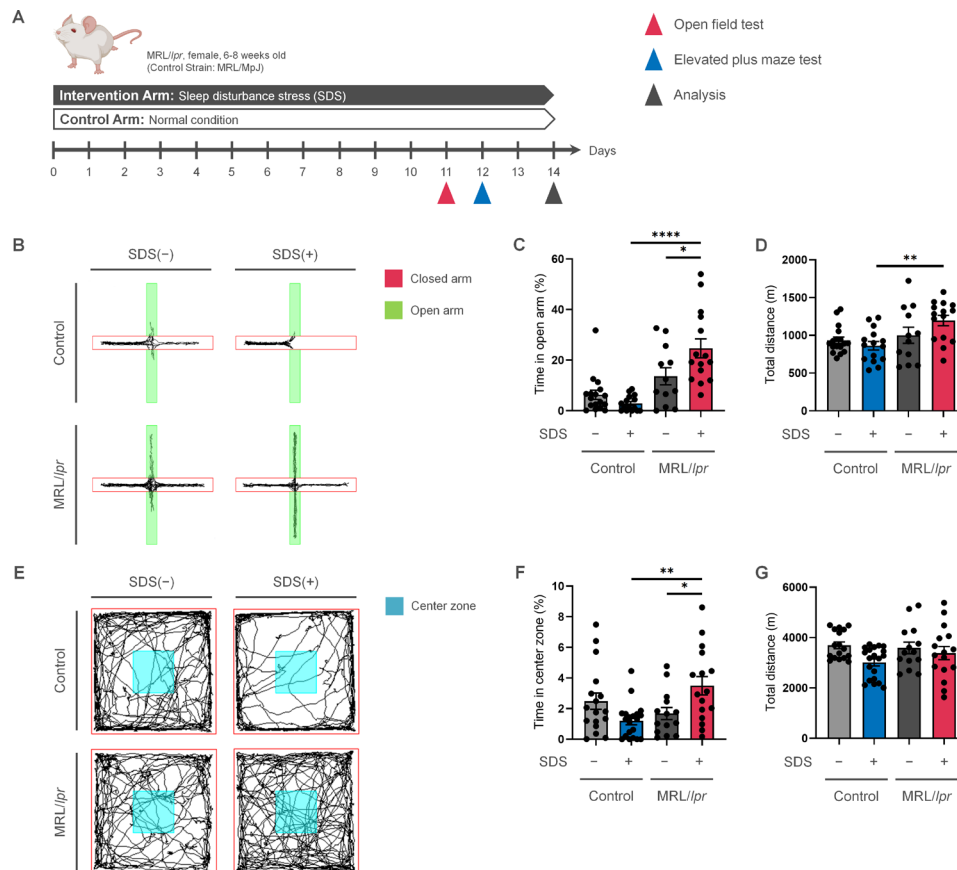


**Figure 1** Stress-elicited abnormal behaviour and mPFC activation in lupus-prone mice. (A) The study protocol for chronic SDS. (B–D) EPM in SDS-subjected or SDS-free MRL/lpr and control mice (MRL/MpJ). (B) representative trajectories. (C) Percentage of time spent in the open arms and (D) total travelled distance to assess anxiety-like behaviour and general locomotor activity, respectively (n=12–17 per group). (E–G) OF results. (E) representative tracking images. (F) Percentage of time spent in the centre zone and (G) total distance travelled to assess anxiety-like behaviour and general locomotor activity, respectively (n=14–20 per group). Data are means±SEM. \*p<0.05, \*\*p<0.01 and \*\*\*\*p<0.0001 using a two-way ANOVA with post-hoc Tukey-Kramer multiple comparison test. ANOVA, analysis of variance; EPM, elevated plus maze test; mPFC, medial prefrontal cortex; OF, open field test; SDS, sleep disturbance stress.

### Persistent neuronal activation in medial prefrontal cortex of stress-subjected MRL/lpr mice

One of the representative brain regions receiving stress stimulus is the paraventricular nucleus (PVN).<sup>17</sup> PVN neurons send axonal projections to the ventral tegmental area (VTA) as the origin of dopaminergic neurons that project to the medial prefrontal cortex (mPFC) and nucleus accumbens (NAc).<sup>18–19</sup> Previous reports demonstrated that acute single stress activates the mPFC and represses anxiety-like behaviour, while chronic stress causes anxiety by inhibiting the mPFC and activating NAc neurons.<sup>20–21</sup> Therefore, we investigated neuronal activity in these regions in the presence or absence of SDS (figure 2A,B). In the PVN, both SDS-subjected strains showed a higher number of phosphorylated cFos (p-cFos)-positive cells than SDS-free mice (online supplemental figure 2A–C). In the VTA, more p-cFos positive cells were observed in SDS-subjected mice than SDS-free mice regardless of the mouse strain (figure 2C–E). In contrast, only SDS-subjected MRL/lpr mice showed elevated neuronal activation in the mPFC (figure 2F–H). Meanwhile, both stressed strains showed more p-cFos positive cells in the NAc compared with SDS-free strains (figure 2I–K). In contrast, among NOD/ShiJcl mouse strain, SDS-subjected mice showed similar number of p-cFos-positive cells to SDS-free mice (online supplemental figure 2D,E). These findings suggest that the mPFC is an important region for anxiolytic effect for disinhibited behaviour

over NAc activation induced-anxious effect in SDS-subjected MRL/lpr mice.

### Enhanced microglia activation signatures in the pFC of stressed MRL/lpr mice

We hypothesised that the stress load alters gene expression profiles in the mPFC of MRL/lpr mice. An RNA-seq transcriptome analysis of the PFC among the strains detected 7952 differentially expressed genes with an absolute FC over 1.5. A principal component analysis revealed a stress-induced effect on the gene expressions corresponding to the mouse strains (figure 3A). Among these genes, 509 genes were significantly upregulated or downregulated in SDS-subjected MRL/lpr mice compared with the other mouse groups (figure 3B). Using these genes, an ingenuity pathway analysis identified pathways associated with inflammatory and neuronal signalling, such as phagosome formation, neuroinflammation, Th1 pathway, G-protein-coupled receptor and cAMP response element binding protein (CREB) signalling (figure 3C, online supplemental figure 3A). Consistently, Gene Ontology and Kyoto Encyclopedia of Genes and Genomes pathway analyses detected pathways related to the positive regulation of cytokine production, G protein-coupled receptor activity and neuroactive ligand receptor interaction (figure 3D, online supplemental figure 3B).

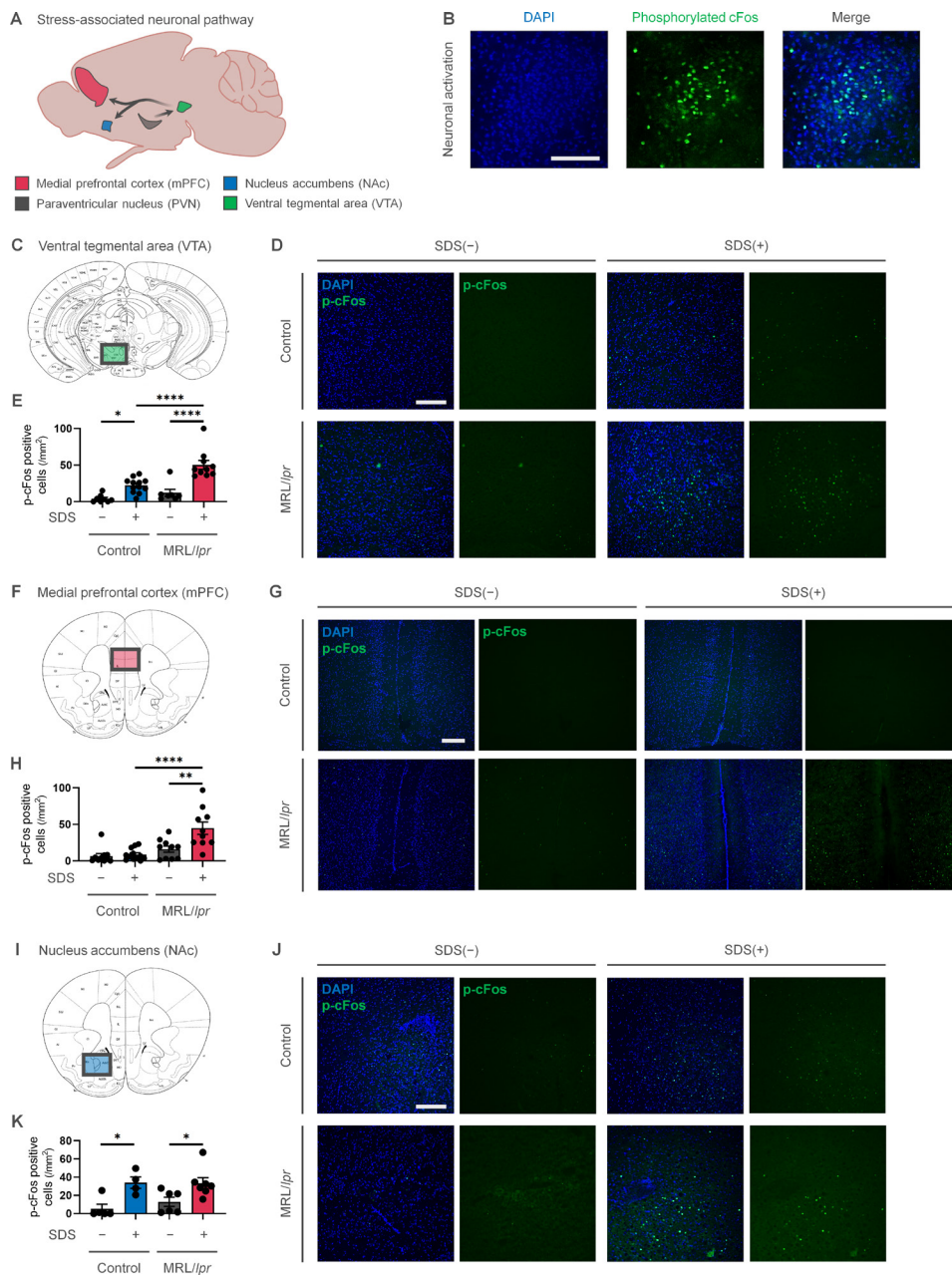


**Figure 2** Neuronal activation of stress-responsive brain regions. (A) The representative stress-responsive neuronal pathway. The PVN sends axonal connections to the VTA, which projects to the mPFC and NAc. (B) Representative images of phosphorylated cFos (p-cFos)-immunostained cells with DAPI. Scale bar: 20  $\mu$ m. (C–K) Evaluation of neuronal activation using immunohistochemistry of p-cFos-positive cells in the (C–E) VTA, (F–H) mPFC and (I) to (K) NAc between SDS-subjected or SDS-free MRL/lpr, and control mice. (C, F and I) Schematic drawings of the VTA, mPFC and NAc were taken from Franklin and Paxinos (1997).<sup>64</sup> (D, G, J) representative immunohistochemical images of activating p-cFos-positive neuronal cells with DAPI in the VTA, mPFC and NAc. Scale bars: (D) and (J) 50  $\mu$ m and (G) 100  $\mu$ m. (H) Quantification of p-cFos-positive cells in the VTA (n=7–12 per group), mPFC (n=10–12 per group), and NAc (n=4–8 per group). Data are means $\pm$ SEM. \*p<0.05, \*\*p<0.01 and \*\*\*\*p<0.0001 using a two-way ANOVA with the post-hoc Tukey-Kramer multiple comparison test. ANOVA, analysis of variance; DAPI, 4',6-diamidino-2-phenylindole; mPFC, medial prefrontal cortex; NAc, nucleus accumbens; p-cFos, phosphorylated cFos; PVN, paraventricular nucleus; VTA, ventral tegmental area.

Considering the inflammatory nature of lupus, we focused on 635 genes associated with the inflammatory pathways analysed above. SDS-subjected MRL/lpr mice demonstrated relatively high expressions for microglia-activating genes, such as *H2-Eb1*, *Nos2*, *Il12b* and *Fcgr4*, and low expressions for microglial-inactivating genes, including *Arg1*, *Nr4a3* and *Trem14* (figure 3E). The *Il12b* gene encodes interleukin 12 (IL-12) p40 subunit, which is shared by IL-12 and IL-23, both of which are critical for inflammation development. We confirmed that *Il12b* gene had the highest expression in the PFC of SDS-subjected

MRL/lpr mice by quantitative PCR (figure 3F). Although the serum IL-12/23p40 level of SDS-subjected MRL/lpr mice was lower than that of SDS-free MRL/lpr mice, the highest CSF IL-12/23p40 protein level was observed in SDS-subjected MRL/lpr mice (figure 3G, online supplemental figure 3C). We also examined the CSF levels of interferon- $\gamma$  and IL-17A, which are IL-12/23p40 signaling-inducible cytokines. The CSF interferon- $\gamma$  and IL-17A tended to be higher levels in SDS-subjected MRL/lpr mice (online supplemental figure 3D,E). Thus, the

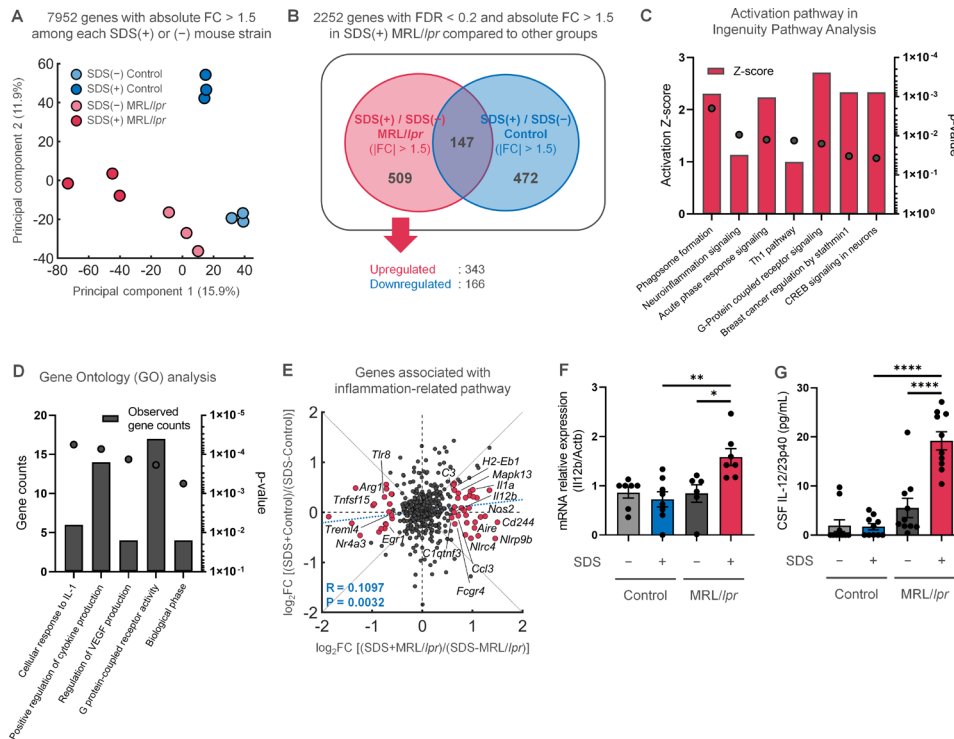


**Figure 3** Upregulation of inflammatory gene expression and IL-12/23p40 level in the PFC of stressed MRL/lpr mice. (A) Principal component analysis of genes with an absolute FC over 1.5 in SDS-subjected or -free strains (n=3 per group). (B) Venn diagram showing the number of stress-affected differentially expressed genes with an absolute FC >1.5 and false discovery rate-corrected p value <0.2 among the mouse groups. SDS-subjected MRL/lpr demonstrated unique expressions of 343 upregulated and 166 downregulated genes compared with SDS-free MRL/lpr mice and control strains. (C) Ingenuity pathway analysis and (D) GO analysis of the 343 differentially upregulated genes from SDS-subjected MRL/lpr mice. Dots represent p values. (E) SDS-induced changes in inflammation-related gene expressions in the PFC of MRL/lpr and controls compared with the respective SDS-free strains. red, SDS-induced MRL/lpr uniquely expressed genes. (R=0.1097, linear regression, Pearson's correlation). (F) *Il12b* mRNA expression relative to SDS-free control mice by quantitative PCR (n=6–8 per group). (G) IL-12/23p40 level in the CSF measured by ELISA (n=10–11 per group). (F, G) data are means±SEM. \*p<0.05, \*\*p<0.01 and \*\*\*\*p<0.0001 using a two-way ANOVA with the post-hoc Tukey-Kramer multiple comparison test. ANOVA, analysis of variance; CSF, cerebrospinal fluid; FC, fold change; GO, Gene Ontology; IL, interleukin; PFC, prefrontal cortex; SDS, sleep disturbance stress.

upregulation of microglial proinflammatory genes, including *Il12b*, in the PFC of SDS-subjected MRL/lpr mice was observed.

### Microglial activation and neuronal alterations in the mPFC of SDS-subjected MRL/lpr mice

We next investigated which cell types produce IL-12/23p40 in the PFC. We first analysed the CNS invasion of CD45<sup>high</sup> immune cells, especially T cells. Although peripheral CD45<sup>high</sup> immune cells were present in the cortex of 14-week-old MRL/lpr mice, as previously described,<sup>22</sup> few CD45<sup>high</sup> cells were detected in the cortex of 8-week-old MRL/lpr mice (online supplemental figure 4A,B). Therefore, we focused on CNS cells responsible for IL-12/23p40 production. Public databases of gene expressions in CNS cells demonstrated that microglia and macrophages express *Il12b* gene (online supplemental figure 4C).<sup>23</sup> Consistently, SDS-subjected MRL/lpr mice had the highest number of Iba-1<sup>+</sup>-activated microglia in the mPFC based on the aggregation of a lysosomal activation marker, CD68, without any microglial density changes (figure 4A–C, online supplemental figures 5A,B). A flow cytometric analysis revealed that IL-12/23p40-positive cortical microglia increased in SDS-subjected MRL/lpr mice (figure 4D,E, online supplemental figure 5C,D). Additionally, mPFC microglia in NOD/ShiJcl mouse strain did not be affected by SDS (online supplemental figure 5E–G). We then investigated which cells receive IL-12/23p40 in the mPFC. Previous reports showed that neurons express IL-12 receptors

and IL-12 enhances neurite outgrowth.<sup>24, 25</sup> Indeed, mPFC neurons expressed IL12Rβ1, a subunit of IL-12/23p40 receptor (online supplemental figure 6A). We further found that Stat4, a downstream molecule of IL-12/23 signalling, was highly phosphorylated in the PFC neurons of SDS-subjected MRL/lpr mice (figure 4F,G, online supplemental figure 6B,C). Phosphorylation of Stat3, another downstream molecule of IL-12/23 signalling, was not significantly affected by SDS in the PFC neurons of SDS-subjected MRL/lpr mice (online supplemental figure 6D–F), indicating mainly activated IL-12 signalling in the PFC neurons. Furthermore, SDS-subjected MRL/lpr mice had the most abnormal spines in proximal dendrites to soma of mPFC neurons (figure 4HI), where few dendritic spines are generally expressed.<sup>26</sup> We also observed that MRL/MpJ control mice stereotaxically injected with recombinant IL-12/23p40 demonstrated more abnormal dendritic spines in mPFC neurons (online supplemental figure 6G,H). Therefore, we detected IL-12/23p40 upregulation in activated microglia and Stat4-mediated neuronal alterations in the mPFC of SDS-subjected MRL/lpr mice.

### Cancelling neuropsychiatric phenotypes in stressed MRL/lpr mice by IL-12/23p40 neutralisation and tyrosine kinase 2 inhibition

To investigate whether the blockade of IL-12/23p40 signalling ameliorates the stress-elicited phenotypes in MRL/lpr mice, we

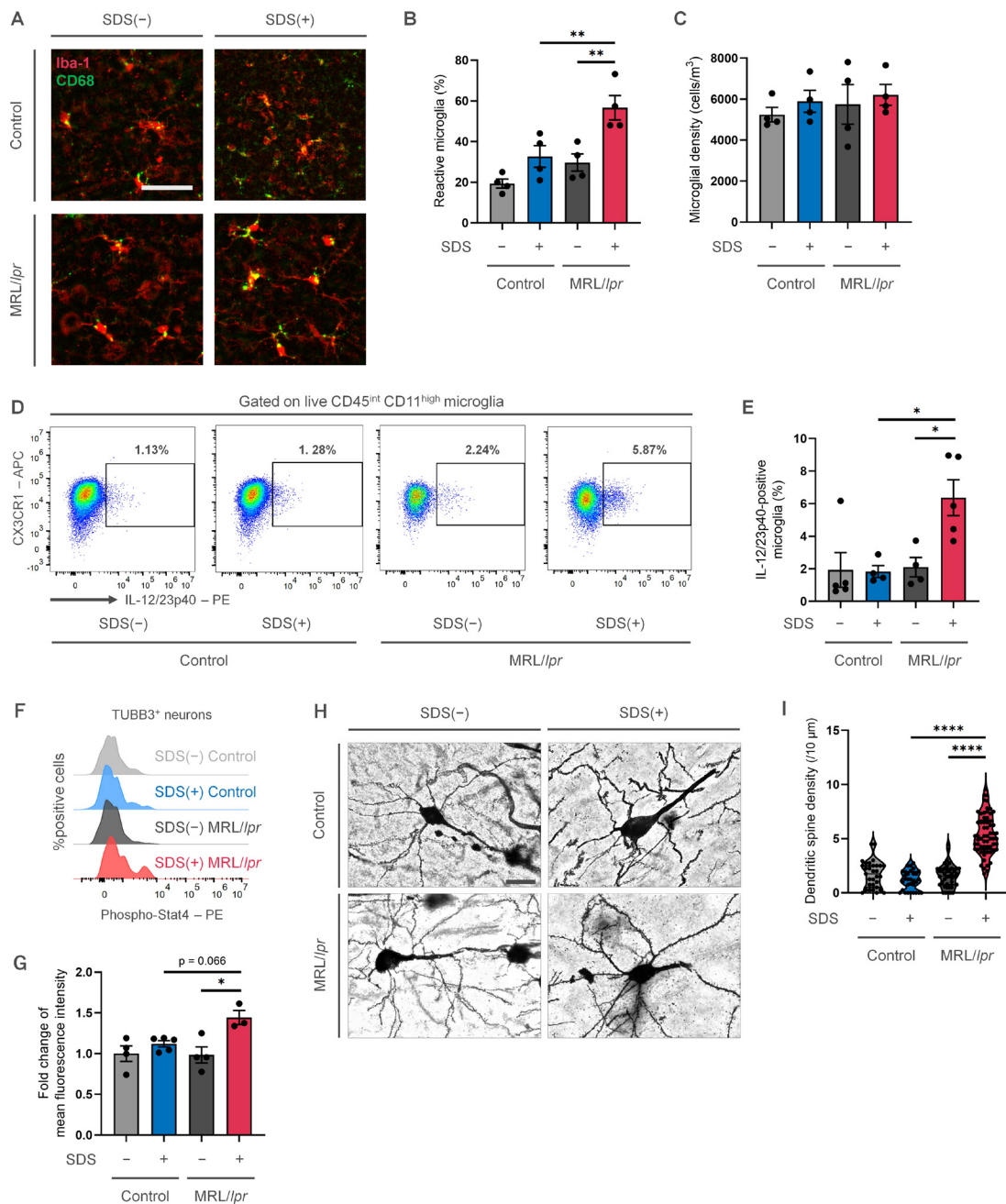


**Figure 4** Microglial activation with IL-12/23p40 upregulation and dendritic alterations in stressed MRL/lpr mice. (A–C) Microglial activation state analysis in the mPFC. (A) Representative immunohistochemical images of Iba-1-positive microglia with a CD68 lysosomal marker. (B) Percentage of reactive microglia and (C) microglial density (n=4 per group). (D–E) Flow cytometric analysis for IL-12/23p40 production from live CD45<sup>int</sup>CD11b<sup>high</sup>CX3CR1<sup>+</sup> cortical microglia. (D) Representative gating for IL-12/23p40-positive microglia. (E) Percentage of IL-12/23p40-producing microglia (n=4–5 per group). (F and G) Phosphorylated-Stat4 expression in TUBB3<sup>+</sup> neurons measured by flow cytometry. (F) Representative histogram for phosphorylated-Stat4 and (G) FC of the mean fluorescence intensity for the phosphorylated-Stat4 expression relative to SDS-free control mice (n=4–5 per group). (H–I) Golgi-Cox staining of neurons in the mPFC. (H) Representative images of layer 2/3 pyramidal neurons. (I) Quantification of the dendritic spine density proximal to the soma of layer 2/3 pyramidal neurons (n=31–62 dendrites per group). Scale bars: (A) 50  $\mu$ m and (K) 20  $\mu$ m. (B), (C), (E) and (G) Data are means $\pm$ SEM. or (I) medians (IQR). \*p<0.05, \*\*p<0.01 and \*\*\*\*p<0.0001 using a two-way ANOVA with the Tukey-Kramer test. ANOVA, analysis of variance; FC, fold change; IL, interleukin; mPFC, medial prefrontal cortex; SDS, sleep disturbance stress.

intracerebroventricularly infused IL-12/23p40 neutralising antibody in SDS-subjected MRL/lpr mice (figure 5A). The infused immunoglobulin G (IgG) successfully reached the mPFC, and IL-12/23p40 antibody reduced the CSF IL-12/23p40 level without any change in the serum level of IL-12/23p40 or spleen weight (figure 5B, online supplemental figure 7A–C). Indeed, IL-12/23p40 blockade in the CNS ameliorated stress-induced anxiolytic behaviour (figure 5C–E). Moreover, microglial

activation and phosphorylated Stat4 levels in the mPFC were reduced (online supplemental figure 7D–F). The abnormal increase of proximal dendritic spines was also remedied (figure 5F,G).

We next employed deucravacitinib, a clinically applied selective inhibitor of tyrosine kinase 2 (Tyk2), which is an IL-12/23p40 downstream intracellular signalling kinase.<sup>27</sup> We found that Tyk2 inhibitor treatment reduced the spleen weight (figure 6A–C)

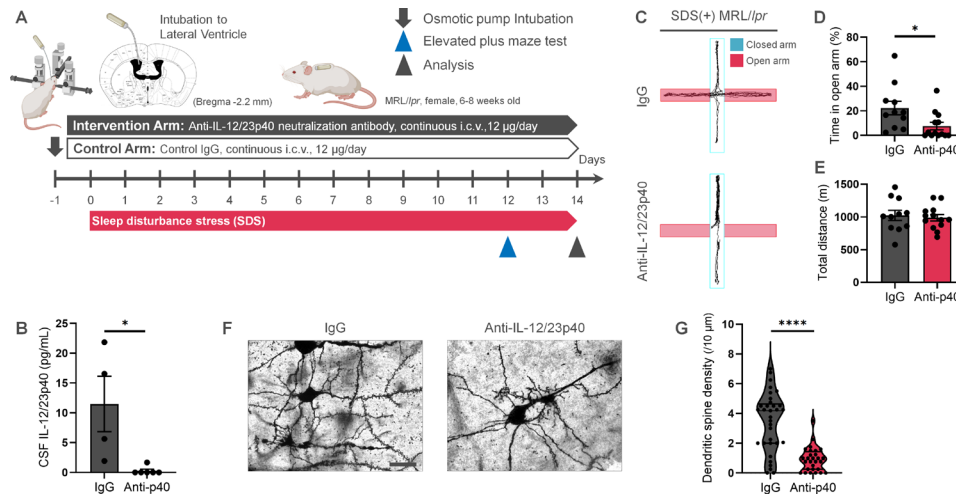


**Figure 5** Cancellation of stress-elicited phenotypes in MRL/lpr by neutralising antibody-mediated IL-12/23p40 signalling blockade. (A) Schematic representation of the CNS-targeted IL-12/23p40 blockade in SDS-subjected MRL/lpr mice. (B–G) Successful inhibition of SDS-induced neuropsychiatric phenotypes by IL-12/23p40 depletion. (B) ELISA for IL-12/23p40 concentration in the CSF (n=4–6 per group). (C) Representative tracks, (D) percentage of time spent in the open arm and (E) total travelled distance in the EPM (n=11 to 13 per group). (F) Representative Golgi-Cox staining of layer 2/3 pyramidal neurons in the mPFC. (G) Quantification of the spinal density of proximal dendrites to soma (n=28–33 dendrites per group). (F) scale bar, 20 µm. (B), (D) and (E) Data are means±SEM or (G) medians (IQR). \*p<0.05 and \*\*\*\*p<0.0001 using an unpaired Student's t-test. CSF, cerebrospinal fluid; CNS, central nervous system; EPM, elevated plus maze test; IgG, immunoglobulin G; IL, interleukin; mPFC, medial prefrontal cortex; SDS, sleep disturbance stress.

and suppressed cortical microglial activation with IL-12/23p40 production, phosphorylation of Stat4 in cortical neurons, and anxiolytic behaviour without any effects on general locomotor activity, and increased the number of spines in proximal dendrites (figure 6D–N, online supplemental figure 8). Thus, blockade of the IL-12/23p40-Tyk2 signalling pathway in the CNS successfully inhibited the stress-induced neuropsychiatric phenotypes in SDS-subjected MRL/lpr mice.

### High IL-12/23p40 levels in the CSF and mPFC atrophy in patients with dNPSLE

To investigate whether IL-12/23p40 in the CNS affects the pathogenesis of dNPSLE, we measured IL-12/23p40 levels in the CSF and serum of healthy controls and lupus patients with active disease (figure 7A). In the Hokkaido University Hospital cohort, including patients with dNPSLE and patients with SLE without diffuse neuropsychiatric symptoms (non-dNPSLE), which include fNPSLE (online supplemental table 1), CSF IL-12/23p40 levels were highest in patients with dNPSLE, whereas serum levels were similar among all groups (figure 7B, online supplemental figure 9A). Although statistical difference was not observed due to the small number of patients with dNPSLE, the patients without treatment tended to show higher levels of CSF IL-12/23p40 than those treated with glucocorticoid combined with immunosuppressants, suggesting that high variance of CSF IL-12/23p40 levels was likely caused by therapeutic effects of immunosuppressants (online supplemental figure 9B). The CSF IL-12/23p40 level had high diagnostic utility for dNPSLE, with an AUC of 0.8438 (95% CI 0.7377 to 0.9498, sensitivity 78% and specificity 88%) (figure 7C). Using the Kitasato University Hospital cohort (online supplemental table 2), we validated these results, as the higher CSF levels of IL-12/23p40 in patients with dNPSLE than fNPSLE and good diagnostic efficacy for dNPSLE with an AUC of 0.7346 (95% CI 0.5472 to 0.9220, sensitivity 61% and specificity 78%) (figure 7D–E, online supplemental figure 9C). Notably, the patients with ACS or psychosis occupied 70%–80% of the dNPSLE population, and there were few

patients with anxiety in both cohorts (online supplemental tables S1 and S2). We investigated the CSF IL-12/23p40 level of the patients with primary SS as a disease control. The IL-12/23p40 levels were significantly higher in the CSF of patients with dNPSLE than that of patients with primary SS (online supplemental figure 9D).

We next investigated morphological changes of the brain in patients with dNPSLE and patients with non-dNPSLE by VBM using another Hokkaido University cohort (figure 7A and online supplemental table 3). The patients with dNPSLE showed less volumes of total grey matter and WM, and more WM lesions than patients with non-dNPSLE (figure 7F, online supplemental figure 9E–H). Based on the results of the SDS mouse model, we calculated the mPFC volume and atrophic Z-score using an age-matched healthy control dataset as a reference, finding a larger mPFC volume reduction with higher Z-score in patients with dNPSLE than patients with non-dNPSLE despite a similar frontal cortex volume (figure 7H1, online supplemental figure 9I). In the Hokkaido University Hospital cohort (online supplemental table 1), patients with dNPSLE received more sleep medications than patients with non-dNPSLE (20/28, 71% vs 6/19, 32%, p=0.0064) at the perioperative period of the CSF collection without any statistical difference in the glucocorticoid dose (online supplemental table 1 and 4). These might indicate a high prevalence of sleep disorder on dNPSLE onset. Together, these results as patients with dNPSLE have increased IL-12/23p40 levels in the CSF and mPFC atrophy, possibly being linked to the results of our mouse model.

### DISCUSSION

Previous studies have reported that chronic stress inhibits PFC function with a decreasing density of dendritic spines, impairing behavioural flexibility, including more anxiety-like behaviours.<sup>20 21 28–31</sup> Contrary to these reports, our results demonstrated that stressed lupus-prone mice showed PFC impairment with increasing dendritic spinal density and disinhibited risk-taking and less anxiety-like behaviours. We further

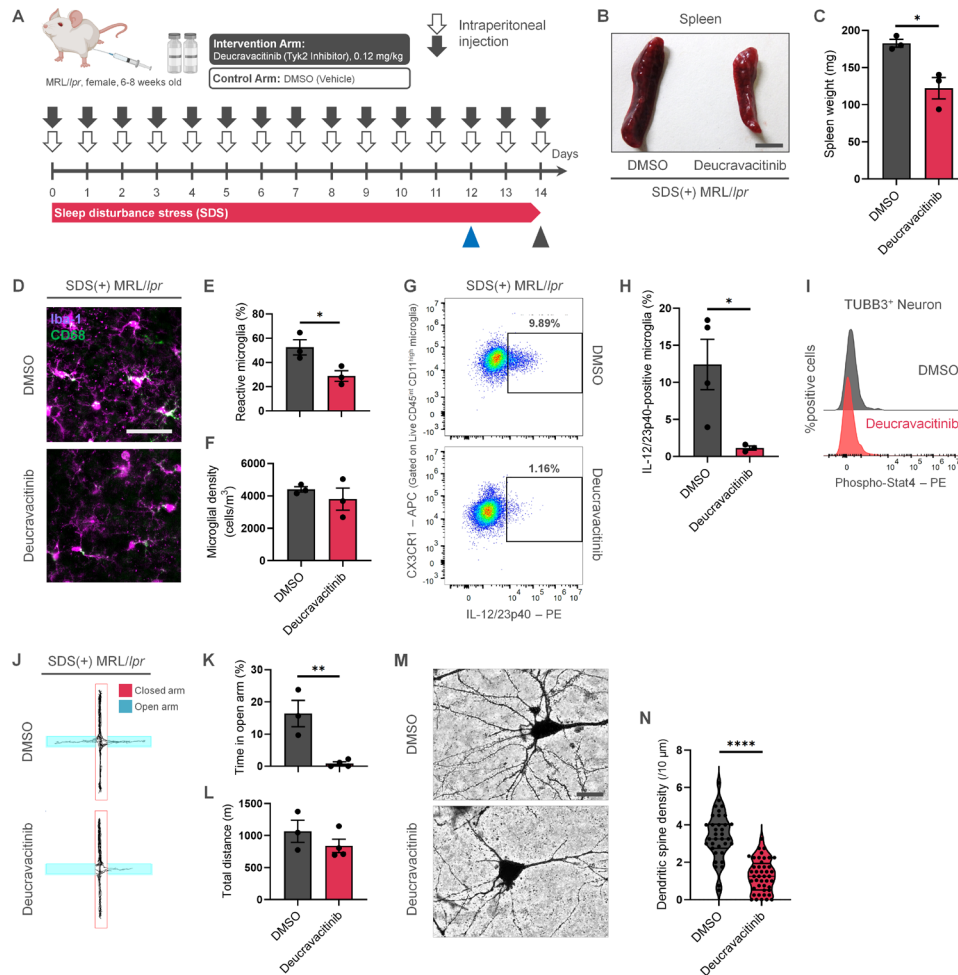


**Figure 6** Improvement of stress-elicited neuropsychiatric phenotypes in lupus-prone mice with Tyk2 inhibitor. (A) The experimental protocol for the systemic administration of deucravacitinib in SDS-subjected MRL/lpr mice. (B–N) SDS-elicited phenotypes were cancelled by deucravacitinib. (B) Macroscopic findings of the spleen. (C) Spleen weight comparison (n=3 per group). (D) Representative images of activated microglia. (E) Percentage of reactive microglia and (F) microglial density (n=3 per group). (G) Representative gating for IL-12/23p40<sup>+</sup> microglia and (H) its percentage (n=3 per group). (I) Histogram of phosphorylated-Stat4 expression in TUBB3<sup>+</sup> neurons. (J) Representative trajectories, (K) percentage of time spent in the open arm and (L) total distance in the EPM (n=3–4 per group). (M) Representative images of layer 2/3 pyramidal neurons in the mPFC. (N) Quantification of the proximal dendritic spine density (n=35–44 dendrites per group). Scale bars: (B) 10 mm, (D) 50  $\mu$ m and (M) 20  $\mu$ m. Data are means $\pm$ SEM except (N) which shows medians (IQR). \*p<0.05, \*\*p<0.01 and \*\*\*\*p<0.0001 using an unpaired Student’s t-test. DMSO, dimethyl sulfoxide; EPM, elevated plus maze test; IL, interleukin; mPFC, medial prefrontal cortex; SDS, sleep disturbance stress; Tyk2, tyrosine kinase 2.

showed that the stress-induced activation of microglia in the mPFC plays a key role.

It is well known that activated microglia induce neuroinflammation, predisposing susceptible individuals to neuropsychiatric diseases,<sup>32–34</sup> even though microglia engage with neurons to maintain homeostasis in the CNS.<sup>32–34</sup> In other words, in a pathological state, activated microglia potentially exacerbate neurological diseases by dysregulating neural circuits.<sup>35–36</sup> For instance, homeostatic microglia drive negative feedback mechanisms to inhibit neuronal activation via extracellular ATP to protect the brain from excessive activation, while activated proinflammatory microglia do not trigger these negative feedback mechanisms.<sup>37</sup> In addition, activated microglia alter neuronal functions and eliminate dendritic spines in pyramidal neurons of the mPFC.<sup>38–39</sup> Moreover, microglia from lupus-prone mice exhibit an activated phenotype with upregulated inflammation-related genes, including *Il12b*, and cause neuronal dysfunction leading to neuroinflammation and microglial phagocytosis.<sup>40–41</sup> Although some microglia populations protect lupus model mice from neurodegeneration,<sup>42–43</sup> activated microglia also induce

impairment of the blood–brain barrier to cause neuroinflammation development.<sup>44</sup> Thus, it is reasonable that activated microglia can induce the abnormal activation of neuronal circuits in the mPFC to cause neuropsychiatric phenotypes in stressed MRL/lpr mice. Although stress is known to induce microglial activation via the norepinephrine- $\beta$  adrenergic receptor signaling pathway,<sup>45–46</sup> the molecular mechanisms causing the microglial activation in SDS-subjected MRL/lpr mice are unknown at present. In addition, the behavioural testing results had relatively high variance in stressed-MRL/lpr mice, possibly being derived from the variance of disease penetrance. Further research for understanding the molecular mechanisms of stress-induced microglial activation and neuronal alteration in lupus-prone condition is required.

IL-12/23p40 is a subunit that dimerises with IL-12p35 or IL-23p19 to form IL-12 and IL-23.<sup>47</sup> In autoimmune disorders, IL-12 and IL-23 are associated with the pathogenesis predominantly through T cell-mediated immunity. While some studies reported that IL-12 can relieve neuroinflammation in an EAE model,<sup>48–49</sup> previous research also demonstrated that IL-12 and



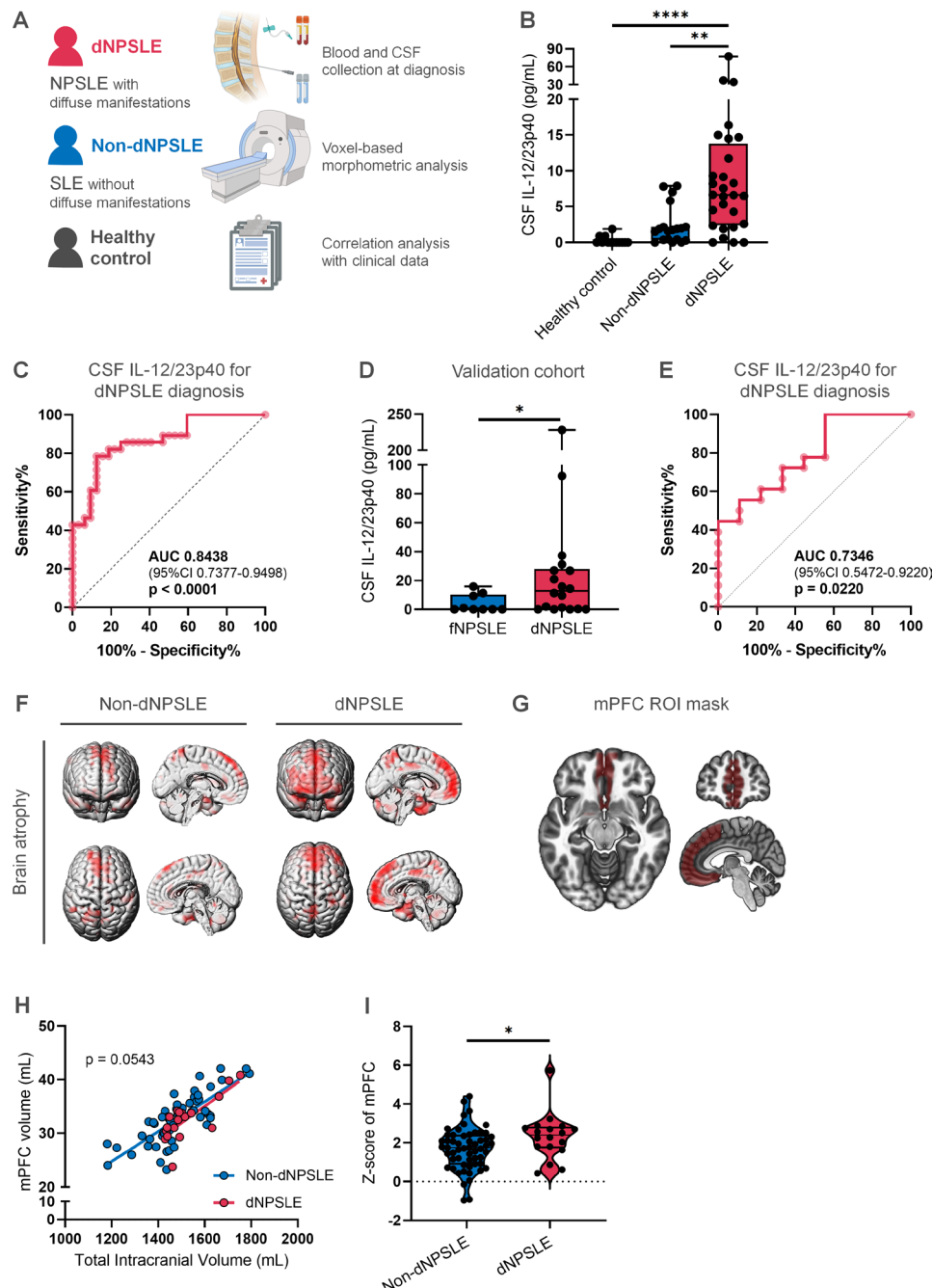


**Figure 7** IL-12/23p40 upregulation and mPFC atrophy in patients with NPSLE with diffuse manifestations (dNPSLE). (A) Schema for the evaluation of human clinical samples and data. (B) and (C) The derivation cohort of patients with SLE and HCs at Hokkaido University Hospital. (B) CSF IL-12/23p40 level measured by ELISA (n=13 HCs, n=19 non-dNPSLE and n=28 dNPSLE). (C) An ROC analysis of CSF IL-12/23p40 levels for dNPSLE diagnosis. (D) and (E) The validation cohort of patients with NPSLE at Kitasato University hospital. (D) CSF IL-12/23p40 levels (n=9 fNPSLE and n=18 dNPSLE). (E) An ROC analysis of the CSF IL-12/23p40 level for dNPSLE classification. (F) Representative brains with atrophy rendered on the reference anatomical brain view against the IXI reference dataset. (G) Used brain ROI mask of the mPFC, rendered as red. (H) Correlation between the mPFC volume and TIV (blue, n=57 non-dNPSLE; red, n=18 dNPSLE). (I) Z-scores of mPFC atrophy against the IXI reference dataset. (B), (D) and (I) Data are medians (IQR). \* $p < 0.05$ , \*\* $p < 0.01$  and \*\*\*\* $p < 0.0001$  using (B) the Kruskal-Wallis test with the post-hoc Steel-Dwass method, (D) and (I) Mann-Whitney U test and (H) ANCOVA adjusting for TIV, age, sex and disease duration of SLE. ANCOVA, analysis of covariance; CSF, cerebrospinal fluid; CNS, central nervous system; dNPSLE, diffuse neuropsychiatric systemic lupus erythematosus; EPM, elevated plus maze test; HCs, healthy controls; IgG, immunoglobulin G; IL, interleukin; mPFC, medial prefrontal cortex; NPSLE, neuropsychiatric systemic lupus erythematosus; ROC, receiver operating characteristic; ROI, region of interest; SDS, sleep disturbance stress; SLE, systemic lupus erythematosus; TIV, total intracranial volume.

IL-23 can exacerbate neuroinflammation in EAE.<sup>50,51</sup> They also exacerbate the pathology of Alzheimer's disease.<sup>52</sup> We showed that IL-12/23p40 mainly expressed from activated microglia alter mPFC neurons, modifying the neuronal structure as previously demonstrated.<sup>24</sup> A phase 3 clinical trial for ustekinumab,

an IL-12/23p40 neutralisation antibody, in patients with SLE was discontinued due to poor efficacy (Ustekinumab Press Release).<sup>53</sup> However, considering that patients with NPSLE were excluded from the trial, whether this antibody or the Tyk2 inhibitor has efficacy in patients with dNPSLE should be explored.

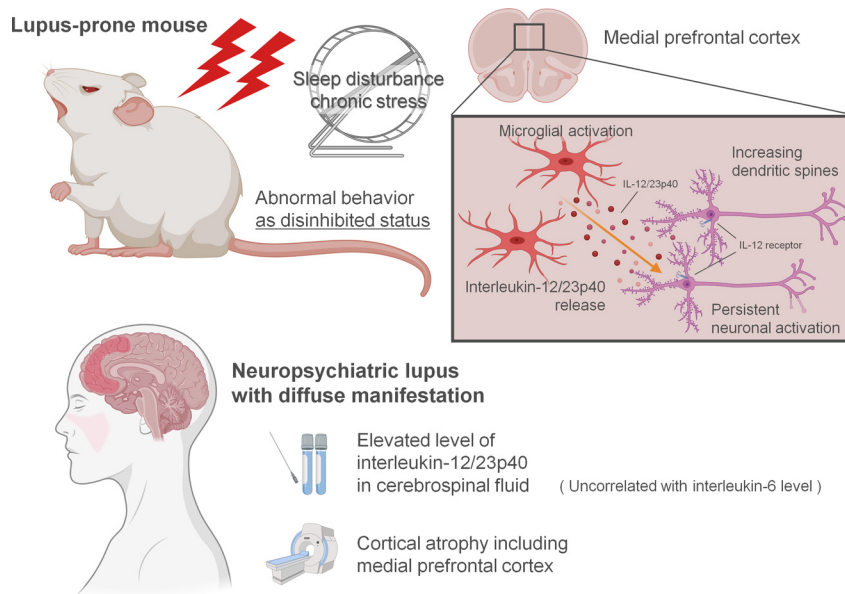


**Figure 8** Graphical abstract. SDS-subjected lupus-prone MRL/lpr mice demonstrated disinhibited anxiolytic behaviour. Mechanistically, microglial activation, IL-12/23p40 upregulation and neuronal activation with increasing dendritic spines in the medial prefrontal cortex were observed. These stress-induced neuropsychiatric phenotypes were reversed by blockade of the IL-12/23 axis using IL-12/23p40 neutralising antibody or Tyk2 inhibitor. Patients with neuropsychiatric lupus showing diffuse neuropsychological manifestations demonstrated elevated levels of IL-12/23p40 in the cerebrospinal fluid and medial prefrontal cortical atrophy. These results suggest a pathological link between the stress-induced microglial IL-12/23p40 axis with neuronal activation and the development of neuropsychiatric lupus with diffuse manifestations. IL, interleukin; SDS, sleep disturbance stress; Tyk2, tyrosine kinase 2.

As a possible molecular mechanism of dNPSLE, we hypothesised that stress-induced microglial activation, which led to an overactivation of neurons in the mPFC; this overactivation is critical for disinhibited symptoms like agitation, psychosis and ACS. Our study demonstrated that chronic stress induced a risk-taking behaviour with mPFC overactivation in SDS-subjected MRL/lpr mice, which would be similar behaviours to the hyperactivity and psychomotor agitation in patients with NPSLE. Indeed, a specific type of delirium with increased vigilance manifesting agitation, overactivity and hallucinations is observed in patients with NPSLE with ACS. Our mouse model could at least in part explain some of these ACS manifestations as stress-induced and inflammation-induced mPFC overactivation in patients with dNPSLE. Consistently, patients with SLE show an altered mPFC status in decision-making tasks,<sup>54</sup> reduced metabolism and atrophy,<sup>55</sup> and decreased cerebral blood flow.<sup>56</sup> An increase of dendritic spines in PFC neurons is also observed in autism-spectrum disorder and in patients taking antidepressants or N-methyl-D-aspartic acid, which manifest anxiolytic/depressive hyperactive behaviour.<sup>57–60</sup>

Patients with SLE often show more exasperated neuropsychiatric symptoms just after receiving glucocorticoid therapy compared with patients with other autoimmune disorders. These post-glucocorticoid neuropsychiatric symptoms are similar to the diffuse manifestations in NPSLE.<sup>61</sup> Because glucocorticoids sometimes induce mPFC impairment via neuronal alterations,<sup>62,63</sup> IL-12/23 signalling in the altered microglia-neuronal axis in the mPFC demonstrated here may contribute to the development of neuropsychiatric symptoms in patients with SLE undergoing glucocorticoid treatment. Compared with glucocorticoid monotherapy, we thus hypothesise that immunosuppressants such as cyclophosphamide, which would induce microglial apoptosis, combined with glucocorticoid possibly works better for dNPSLE symptoms through inhibiting the interaction between activated microglia and neurons described here. Moreover, JAK/Tyk2-Stat

inhibitors would be beneficial for dNPSLE through inhibiting activated microglia-inducing neuronal alteration.

Taken together, we demonstrate that stress has pathogenic neuropsychiatric effects on a lupus rodent model by activating microglia and altering neurons in the mPFC via the IL-12/23 signalling pathway. We also found similar phenomena as an elevated level of CSF IL-12/23p40 and mPFC atrophy in patients with dNPSLE (figure 8). Therefore, our findings suggest that IL-12/23p40 in the mPFC is a therapeutic target for dNPSLE.

#### Author affiliations

- <sup>1</sup>Division of Molecular Psychoimmunology, Institute for Genetic Medicine, Graduate School of Medicine, Hokkaido University, Sapporo, Japan
- <sup>2</sup>Department of Rheumatology, Endocrinology and Nephrology, Faculty of Medicine and Graduate School of Medicine, Hokkaido University, Sapporo, Japan
- <sup>3</sup>Group of Quantum Immunology, Institute for Quantum Life Science, National Institute for Quantum and Radiological Science and Technology, Inage, Japan
- <sup>4</sup>Center for Infectious Cancers, Institute for Genetic Medicine, Hokkaido University, Sapporo, Japan
- <sup>5</sup>Division of Molecular Neuroimmunology, National Institute for Physiological Sciences, National Institute of Natural Sciences, Okazaki, Japan
- <sup>6</sup>Department of Rheumatology and Infectious Diseases, School of Medicine, Kitasato University, Sagami, Japan
- <sup>7</sup>Department of Immunology, National Institute of Neuroscience, National Center of Neurology and Psychiatry, Kodaira, Japan
- <sup>8</sup>Department of Diagnostic and Interventional Radiology, Hokkaido University Hospital, Sapporo, Japan
- <sup>9</sup>Global Center for Biomedical Science and Engineering, Faculty of Medicine, Hokkaido University, Sapporo, Japan
- <sup>10</sup>Department of Anatomy, Faculty of Medicine, Hokkaido University, Sapporo, Japan

**Acknowledgements** We thank Ms Yumiko Kaneko, Ms Yui Ishikura, Mr Yusuke Fujita and Ms Chiemi Nakayama for their experimental support, and Dr Yasuhiro Hasegawa (Kitasato University) for collecting the clinical data. We are grateful to Dr Peter Karagiannis (Center for iPS Cell Research and Application, Kyoto University, Kyoto) for reading the manuscript. We also appreciate BioRender.com for the support of drawing figures.

**Contributors** Conceptualisation: NA and MM. Methodology: NA, NT, YF, YT, RH and KKT. Investigation: NA, NT, MT, KK, MU and KKT. Visualisation: NA and YF. Resources: YA, WS, KKT and MY. Funding acquisition and project administration: KO,

TA and MM. Supervision: MKono, MKato, MY, MW, TA and MM. Writing—original draft: NA, YF and KO. Writing—review and editing: OA, KKT, MW, TA and MM. Guarantors: TA and MM.

**Funding** This work was funded by the grant from Bristol Myers Squibb Foundation to TA, and grants from JSPS KAKENHI, Q-Leap (JPMXS0120330644), AMED, The Joint Usage/Research Center Institute for Genetic Medicine, Hokkaido University, the Photo-excitonix Project at Hokkaido University and the Promotion Project for Young Investigators at Hokkaido University to MM.

**Competing interests** None declared.

**Patient and public involvement** Patients and/or the public were not involved in the design, or conduct, or reporting, or dissemination plans of this research.

**Patient consent for publication** Not applicable.

**Ethics approval** This study involves human participants. Ethical approval for the clinical studies was granted by institutional review board of Hokkaido University Hospital (approval numbers: 019-0055 and 020-0110) and that of Kitasato University School of Medicine (approval number: B20-231) and for the animal experiments and clinical studies was granted by the Institutional Animal Care and Use Committees of Hokkaido University (approval number: 14-0083). This study complied with the Declaration of Helsinki. Participants gave informed consent to participate in the study before taking part.

**Provenance and peer review** Not commissioned; externally peer reviewed.

**Data availability statement** Data are available in a public, open access repository. Data are available upon reasonable request. In detail, RNA-seq datasets that support the observations of this study have been deposited in the Gene Expression Omnibus with the series accession number GSE176429. MRI data have been stored locally following national and Japanese laws on the protection of individuals with regard to the processing of personal data. Other data are available in the main text or the supplementary materials and are available upon reasonable request to the corresponding author.

**Supplemental material** This content has been supplied by the author(s). It has not been vetted by BMJ Publishing Group Limited (BMJ) and may not have been peer-reviewed. Any opinions or recommendations discussed are solely those of the author(s) and are not endorsed by BMJ. BMJ disclaims all liability and responsibility arising from any reliance placed on the content. Where the content includes any translated material, BMJ does not warrant the accuracy and reliability of the translations (including but not limited to local regulations, clinical guidelines, terminology, drug names and drug dosages), and is not responsible for any error and/or omissions arising from translation and adaptation or otherwise.

#### ORCID iDs

Nobuya Abe <http://orcid.org/0000-0001-8644-1007>  
 Yuichiro Fujieda <http://orcid.org/0000-0003-4705-341X>  
 Michihito Kono <http://orcid.org/0000-0002-7663-534X>  
 Masaru Kato <http://orcid.org/0000-0002-2023-6585>  
 Yoshiyuki Arinuma <http://orcid.org/0000-0003-1305-991X>  
 Masaaki Murakami <http://orcid.org/0000-0001-7159-7279>

#### REFERENCES

- Kaul A, Gordon C, Crow MK, *et al.* Systemic lupus erythematosus. *Nat Rev Dis Primers* 2016;2:16039.
- Jeltsch-David H, Muller S. Neuropsychiatric systemic lupus erythematosus: pathogenesis and biomarkers. *Nat Rev Neurol* 2014;10:579–96.
- Schwartz N, Stock AD, Putterman C. Neuropsychiatric lupus: new mechanistic insights and future treatment directions. *Nat Rev Rheumatol* 2019;15:137–52.
- Hanly JG, Urowitz MB, Su L, *et al.* Prospective analysis of neuropsychiatric events in an international disease inception cohort of patients with systemic lupus erythematosus. *Ann Rheum Dis* 2010;69:529–35.
- Hanly JG. Diagnosis and management of neuropsychiatric SLE. *Nat Rev Rheumatol* 2014;10:338–47.
- Kamimura D, Tanaka Y, Hasebe R, *et al.* Bidirectional communication between neural and immune systems. *Int Immunol* 2020;32:693–701.
- McEwen BS. Physiology and neurobiology of stress and adaptation: central role of the brain. *Physiol Rev* 2007;87:873–904.
- Silva RH, Abilio VC, Takatsu AL, *et al.* Role of hippocampal oxidative stress in memory deficits induced by sleep deprivation in mice. *Neuropharmacology* 2004;46:895–903.
- Youngblood BD, Zhou J, Smagin GN, *et al.* Sleep deprivation by the "flower pot" technique and spatial reference memory. *Physiol Behav* 1997;61:249–56.
- Arima Y, Ohki T, Nishikawa N, *et al.* Brain micro-inflammation at specific vessels dysregulates organ-homeostasis via the activation of a new neural circuit. *Elife* 2017;6:e25517.
- Gangwisch JE, Malaspina D, Boden-Albala B, *et al.* Inadequate sleep as a risk factor for obesity: analyses of the NHANES I. *Sleep* 2005;28:1289–96.
- Vgontzas AN, Zoumakis E, Bixler EO, *et al.* Adverse effects of modest sleep restriction on sleepiness, performance, and inflammatory cytokines. *J Clin Endocrinol Metab* 2004;89:2119–26.
- Song H, Fang F, Tomasson G, *et al.* Association of stress-related disorders with subsequent autoimmune disease. *JAMA* 2018;319:2388–400.
- Sharif K, Watad A, Coplan L, *et al.* The role of stress in the mosaic of autoimmunity: an overlooked association. *Autoimmun Rev* 2018;17:967–83.
- Watanabe-Fukunaga R, Brannan CI, Copeland NG, *et al.* Lymphoproliferation disorder in mice explained by defects in Fas antigen that mediates apoptosis. *Nature* 1992;356:314–7.
- Stojanovich L, Zandman-Goddard G, Pavlovich S, *et al.* Psychiatric manifestations in systemic lupus erythematosus. *Autoimmun Rev* 2007;6:421–6.
- Pacak K, Palkovits M, Kopin IJ, *et al.* Stress-Induced norepinephrine release in the hypothalamic paraventricular nucleus and pituitary-adrenocortical and sympathoadrenal activity: in vivo microdialysis studies. *Front Neuroendocrinol* 1995;16:89–150.
- Hung LW, Neuner S, Polepalli JS, *et al.* Gating of social reward by oxytocin in the ventral tegmental area. *Science* 2017;357:1406–11.
- Lammel S, Ion DI, Roeper J, *et al.* Projection-specific modulation of dopamine neuron synapses by aversive and rewarding stimuli. *Neuron* 2011;70:855–62.
- Tanaka K, Furuyashiki T, Kitaoka S, *et al.* Prostaglandin E2-mediated attenuation of mesocortical dopaminergic pathway is critical for susceptibility to repeated social defeat stress in mice. *J Neurosci* 2012;32:4319–29.
- Chaudhury D, Walsh JJ, Friedman AK, *et al.* Rapid regulation of depression-related behaviours by control of midbrain dopamine neurons. *Nature* 2013;493:532–6.
- Ma X, Foster J, Sakic B. Distribution and prevalence of leukocyte phenotypes in brains of lupus-prone mice. *J Neuroimmunol* 2006;179:26–36.
- Zhang Y, Chen K, Sloan SA, *et al.* An RNA-sequencing transcriptome and splicing database of glia, neurons, and vascular cells of the cerebral cortex. *J Neurosci* 2014;34:11929–47.
- Lin H, Hikawa N, Takenaka T, *et al.* Interleukin-12 promotes neurite outgrowth in mouse sympathetic superior cervical ganglion neurons. *Neurosci Lett* 2000;278:129–32.
- Ireland DDC, Reiss CS. Expression of IL-12 receptor by neurons. *Viral Immunol* 2004;17:411–22.
- Spruston N. Pyramidal neurons: dendritic structure and synaptic integration. *Nat Rev Neurosci* 2008;9:206–21.
- Stark GR, Darnell JE. The JAK-STAT pathway at twenty. *Immunity* 2012;36:503–14.
- Liston C, Miller MM, Goldwater DS, *et al.* Stress-Induced alterations in prefrontal cortical dendritic morphology predict selective impairments in perceptual attentional set-shifting. *J Neurosci* 2006;26:7870–4.
- Popoli M, Yan Z, McEwen BS, *et al.* The stressed synapse: the impact of stress and glucocorticoids on glutamate transmission. *Nat Rev Neurosci* 2011;13:22–37.
- McEwen BS, Morrison JH. The brain on stress: vulnerability and plasticity of the prefrontal cortex over the life course. *Neuron* 2013;79:16–29.
- McKlveen JM, Morano RL, Fitzgerald M, *et al.* Chronic stress increases prefrontal inhibition: a mechanism for stress-induced prefrontal dysfunction. *Biol Psychiatry* 2016;80:754–64.
- Giovanoli S, Engler H, Engler A, *et al.* Stress in puberty unmasks latent neuropathological consequences of prenatal immune activation in mice. *Science* 2013;339:1095–9.
- Kreisel T, Frank MG, Licht T, *et al.* Dynamic microglial alterations underlie stress-induced depressive-like behavior and suppressed neurogenesis. *Mol Psychiatry* 2014;19:699–709.
- Nie X, Kitaoka S, Tanaka K, *et al.* The innate immune receptors TLR2/4 mediate repeated social defeat stress-induced social avoidance through prefrontal microglial activation. *Neuron* 2018;99:464–79.
- Cserép C, Pósfai B, Dénes Ádám. Shaping neuronal fate: functional heterogeneity of direct Microglia-Neuron interactions. *Neuron* 2021;109:222–40.
- Bartels T, De Schepper S, Hong S. Microglia modulate neurodegeneration in Alzheimer's and Parkinson's diseases. *Science* 2020;370:66–9.
- Badimon A, Strasburger HJ, Ayata P, *et al.* Negative feedback control of neuronal activity by microglia. *Nature* 2020;586:417–23.
- Wohleb ES, Terwilliger R, Duman CH, *et al.* Stress-Induced neuronal colony stimulating factor 1 provokes microglia-mediated neuronal remodeling and depressive-like behavior. *Biol Psychiatry* 2018;83:38–49.
- Ta T-T, Dikmen HO, Schilling S, *et al.* Priming of microglia with IFN- $\gamma$  slows neuronal gamma oscillations in situ. *Proc Natl Acad Sci U S A* 2019;116:4637–42.
- Nomura A, Noto D, Murayama G, *et al.* Unique primed status of microglia under the systemic autoimmune condition of lupus-prone mice. *Arthritis Res Ther* 2019;21:303.
- Nestor J, Arinuma Y, Huerta TS, *et al.* Lupus antibodies induce behavioral changes mediated by microglia and blocked by ACE inhibitors. *J Exp Med* 2018;215:2554–66.
- Makinde HM, Winter DR, Procissi D, *et al.* A novel Microglia-Specific transcriptional signature correlates with behavioral deficits in neuropsychiatric lupus. *Front Immunol* 2020;11:230.
- Deczkowska A, Keren-Shaul H, Weiner A, *et al.* Disease-Associated microglia: a universal immune sensor of neurodegeneration. *Cell* 2018;173:1073–81.

- 44 Haruwaka K, Ikegami A, Tachibana Y, *et al.* Dual microglia effects on blood brain barrier permeability induced by systemic inflammation. *Nat Commun* 2019;10:5816.
- 45 Wohleb ES, Hanke ML, Corona AW, *et al.*  $\beta$ -Adrenergic receptor antagonism prevents anxiety-like behavior and microglial reactivity induced by repeated social defeat. *J Neurosci* 2011;31:6277–88.
- 46 Sugama S, Takenouchi T, Hashimoto M, *et al.* Stress-Induced microglial activation occurs through  $\beta$ -adrenergic receptor: noradrenaline as a key neurotransmitter in microglial activation. *J Neuroinflammation* 2019;16:266.
- 47 Teng MWL, Bowman EP, McElwee JJ, *et al.* IL-12 and IL-23 cytokines: from discovery to targeted therapies for immune-mediated inflammatory diseases. *Nat Med* 2015;21:719–29.
- 48 Becher B, Durell BG, Noelle RJ. Experimental autoimmune encephalitis and inflammation in the absence of interleukin-12. *J Clin Invest* 2002;110:493–7.
- 49 Gran B, Zhang G-X, Yu S, *et al.* IL-12p35-deficient mice are susceptible to experimental autoimmune encephalomyelitis: evidence for redundancy in the IL-12 system in the induction of central nervous system autoimmune demyelination. *J Immunol* 2002;169:7104–10.
- 50 Kroenke MA, Carlson TJ, Andjelkovic AV, *et al.* IL-12- and IL-23-modulated T cells induce distinct types of EAE based on histology, CNS chemokine profile, and response to cytokine inhibition. *J Exp Med* 2008;205:1535–41.
- 51 Grifka-Walk HM, Giles DA, Segal BM. IL-12-polarized Th1 cells produce GM-CSF and induce EAE independent of IL-23. *Eur J Immunol* 2015;45:2780–6.
- 52 Vom Berg J, Prokop S, Miller KR, *et al.* Inhibition of IL-12/IL-23 signaling reduces Alzheimer's disease-like pathology and cognitive decline. *Nat Med* 2012;18:1812–9.
- 53 Ustekinumab® Press Release. Janssen announces discontinuation of phase 3 Lotus study evaluating ustekinumab in systemic lupus erythematosus, 2020. Available: <https://www.jnj.com/janssen-announces-discontinuation-of-phase-3-lotus-study-evaluating-ustekinumab-in-systemic-lupus-erythematosus> [Accessed 16 Mar 2021].
- 54 Wu B-B, Ma Y, Xie L, *et al.* Impaired decision-making and functional neuronal network activity in systemic lupus erythematosus. *J Magn Reson Imaging* 2018;48:1508–17.
- 55 Mackay M, Vo A, Tang CC, *et al.* Metabolic and microstructural alterations in the SLE brain correlate with cognitive impairment. *JCI Insight* 2019;4:e124002.
- 56 Papadaki E, Kavroulakis E, Bertsias G, *et al.* Regional cerebral perfusion correlates with anxiety in neuropsychiatric SLE: evidence for a mechanism distinct from depression. *Lupus* 2019;28:1678–89.
- 57 Li N, Lee B, Liu R-J, *et al.* mTOR-Dependent synapse formation underlies the rapid antidepressant effects of NMDA antagonists. *Science* 2010;329:959–64.
- 58 Forrest MP, Parnell E, Penzes P. Dendritic structural plasticity and neuropsychiatric disease. *Nat Rev Neurosci* 2018;19:215–34.
- 59 Moda-Sava RN, Murdock MH, Parekh PK, *et al.* Sustained rescue of prefrontal circuit dysfunction by antidepressant-induced spine formation. *Science* 2019;364:eaat8078.
- 60 Holmes SE, Scheinost D, Finnema SJ, *et al.* Lower synaptic density is associated with depression severity and network alterations. *Nat Commun* 2019;10:1529.
- 61 Shimizu Y, Yasuda S, Kako Y, *et al.* Post-steroid neuropsychiatric manifestations are significantly more frequent in SLE compared with other systemic autoimmune diseases and predict better prognosis compared with de novo neuropsychiatric SLE. *Autoimmun Rev* 2016;15:786–94.
- 62 Barsegyan A, Mackenzie SM, Kurose BD, *et al.* Glucocorticoids in the prefrontal cortex enhance memory consolidation and impair working memory by a common neural mechanism. *Proc Natl Acad Sci U S A* 2010;107:16655–60.
- 63 Butts KA, Weinberg J, Young AH, *et al.* Glucocorticoid receptors in the prefrontal cortex regulate stress-evoked dopamine efflux and aspects of executive function. *Proc Natl Acad Sci U S A* 2011;108:18459–64.
- 64 Franklin KBJ, Paxinos G. *The mouse brain in stereotaxic coordinates*. Academic Press, 1997. ISBN: 9780122660702.

## Supplementary Materials for

### Pathogenic neuropsychiatric effect of stress-induced microglial interleukin-12/23 axis in systemic lupus erythematosus

Nobuya Abe, Masato Tarumi, Yuichiro Fujieda, Nobuhiko Takahashi, Kohei Karino, Mona Uchida, Michihito Kono, Yuki Tanaka, Rie Hasebe, Masaru Kato, Olga Amengual, Yoshiyuki Arinuma, Kenji Oku, Wakiro Sato, Khin K. Tha, Miwako Yamasaki, Masahiko Watanabe, Tatsuya Atsumi, Masaaki Murakami

Corresponding to:  
Masaaki Murakami  
Email: [murakami@igm.hokudai.ac.jp](mailto:murakami@igm.hokudai.ac.jp)

Tatsuya Atsumi  
Email: [at3tat@med.hokudai.ac.jp](mailto:at3tat@med.hokudai.ac.jp)

#### **This file includes:**

- Supplementary Patients, Materials and Methods
- Supplementary References
- Supplementary Figures 1 to 9
- Supplementary Tables 1 to 4

## Supplementary Patients, Materials and Methods

### *Mice*

MRL/MpJmsSlc-*lpr/lpr* (MRL/*lpr*) and MRL/MpJmsSlc-*+/+* (MRL/MpJ) mice were purchased from Japan SLC (Tokyo, Japan). MRL/*lpr* mice demonstrate central nervous system (CNS) symptoms by 6-8 weeks of age but subsequently develop systemic inflammation with nephritis after 10 weeks of age.<sup>1</sup> To avoid the effect of systemic inflammation and to consider the frequent occurrence for the development of neuropsychiatric lupus (NPSLE) in women, 6-8-week-old female mice were analyzed for all experiments. NOD/ShiJcl mice were purchased from CLEA Japan (Tokyo, Japan) and were used as disease control mice.

All mice were maintained under specific pathogen-free conditions on a 13-h light, 11-h dark cycle, and food and water were provided *ad libitum* in accordance with the protocols of Hokkaido University.

### *Sleep disturbance stress loading*

To expose mice to sleep disturbance stress (SDS) for the induction of sleep disorder, the mice were set into SDS cages equipped with a running wheel (140 cm in diameter, SW-15-SD, Melquest Co., Japan) for two weeks, which caused the mice to run on the wheel almost all day and receive long-term stress. Food and water were provided *ad libitum*, and paper-chip bedding was replaced every other day. From the seventh to ninth day during the SDS experiment, the rotation frequencies of the running wheel for each mouse were continuously recorded every 1 hour as actograms using a counting interface (CIF-4M, Melquest, Japan) to evaluate circadian rhythm disruption. The running wheel activity was calculated as the ratio of the number of wheel rotations during the activity and rest states. Normal circadian rhythm was assessed using SDS-free control mice set in the normal cage with a running wheel (SW-15S, Melquest, Japan) for the same period as SDS-subjected mice.

### *Mouse samples including serum and cerebrospinal fluid (CSF)*

Upon brain tissue collection from anesthetized mice before phosphate-buffered saline (PBS) perfusion, 0.5 mL of blood was collected from the right submandibular vein and put on ice. The blood was centrifuged at 800 g for 15 minutes at 4 °C, and the supernatant was collected as serum. In the CSF collection, the scalp of PBS-perfused mice was removed, and superficial neck muscles were cut. The atlanto-occipital membrane above the cisterna magna was dried with paper towels and tapped using a 30G needle (BD) to aspirate the CSF. Blood contamination in the CSF was evaluated by placing a white background below the CSF-collected tube, and blood-contaminated CSF was discarded. The serum and CSF were collected and stored at -30 °C until further processing. To evaluate the stress degree, serum from mice before SDS load was also collected.

### *Immunohistochemistry*

Brains were collected from mice after transcardial perfusion with cold PBS and then 10% neutral buffered formalin. Tissue was then immersed in 10% formalin overnight at 4 °C followed by cryoprotection in 30% sucrose for 48 hours at 4 °C. The processed tissue was cryosectioned coronally in 40-50 µm thick slices and collected in PBS. The sections

were blocked with 5% bovine serum albumin (BSA) with 0.3% Triton X-100 for 1 hour at room temperature and then incubated overnight at 4 °C with the following primary antibodies diluted in PBS with 2% BSA and 0.3% Triton X-100: anti-p-cFos (1:1000, D82C12, Cell Signaling Technology), anti-Iba-1 (1:400, 013-27691, Wako, and NB100-1028, Novus Biologicals), anti-CD68 (1:300, MCA1957GA, Serotec), anti-TCR $\beta$  (1:200, 109208, BioLegend), anti-I-A/I-E (1:200, 107614, BioLegend), anti-IL12R $\beta$ 1 (1:100, A1886, ABclonal) and anti-NeuN (1:500, ABN90, Merck). After three washes, secondary Alexa Fluor dye-conjugated antibodies (Invitrogen) were added at 1:200 for 2 hours at room temperature. Slides were mounted in ProLong Diamond Antifade Mountant with DAPI (4',6-diamidino-2-phenylindole) (ThermoFisher Scientific) and imaged using a Keyence inverted fluorescence microscope, BZ-9000 (Keyence, Japan). Z-stack images were processed by full focus image analysis.

#### *RNA sequencing analysis*

After perfusion with 20 mL of cold PBS, the PFC region from mice was mechanically dissected and homogenized using a polytron homogenizer with the ISOSPIN Cell & Tissue RNA Kit (Nippon Gene, Japan) to isolate total RNA. RNA quantity and quality were assessed using an Agilent 2100 Bioanalyzer (Agilent Technologies). All samples whose RNA Integrity Number as RNA quality was 7.5 or higher were proceeded to the subsequent library preparation. PolyA RNA purified from total RNA using oligo(dT) 25 magnetic beads was transcribed into full-length complementary DNA (cDNA) using a SureSelect Strand Specific RNA Library Preparation Kit (G9691A, Agilent Technologies). The processed library was purified using AMPure XP beads (A63880, Beckman Coulter). Sequencing was performed with a HiSeq 2500 (single-read, 2 × 50 bp) sequencer (Illumina). Strand NGS software (Agilent Technologies) was used to align the RNA-seq reads to the mouse reference genome (mm10). Quality control was also assessed using Strand NGS. Aligned reads were then filtered based on a quality threshold ( $\geq 20$ ), and reads failing the quality control threshold were removed. After filtering, the aligned reads including partial reads were normalized and quantified using the DESeq2 algorithm. Matlab (MathWorks, USA) was used to visualize various outputs including the gene expressions, primary component analysis, and Venn diagrams. The gene sets of interest were analyzed by Ingenuity Pathway Analysis (IPA) (QIAGEN, CA), Gene Ontology (GO) analysis (geneontology.org), and KEGG pathway analysis ([www.genome.jp/kegg/](http://www.genome.jp/kegg/)). Gene sets associated with the inflammatory pathway include genes in the neuroinflammation signaling pathway in IPA, positive regulation of cytokine production in the GO biological process, and cytokine-cytokine receptor interaction pathway in the KEGG pathway.

#### *Quantitative real-time PCR (qPCR)*

cDNA was synthesized from isolated RNA using SuperScript VILO (Invitrogen). The transcript levels were measured with the Applied Biosystems 7500 Real-Time PCR System and TaqMan Minor Groove Binder probes specific for the genes *Il12b* (Mm01288989\_m1) and *Actb* (Mm02619580\_g1). The *Il12b* expression level was compared using the  $\Delta\Delta C_t$  method normalized to *Actb*.

#### *Enzyme-linked immunosorbent assay (ELISA)*

Mouse serum and CSF samples were used to measure interleukin (IL)-12/23p40 with the Mouse IL-12/IL-23p40 ELISA Kit (BioLegend) according to the manufacturer's instructions. To assess the degree of psychophysiological stress, sera were collected from mice before and after SDS load to measure the serum corticosterone level using a Corticosterone ELISA Kit (Cayman Chemical, USA). IL-12/23p40 was measured in human serum and CSF samples with the BD OptEIA Human IL-12 (p40) Kit following the recommendations of the manufacturer.

#### *Multiplex cytokine beads assay*

Mouse CSF was analyzed using the Bio-Plex Pro Mouse Cytokine Assay (Bio-Rad) with the analytes including interferon- $\gamma$  and IL-17A. Data were acquired on a Luminex 200 xPONENT System (Merck KGaA).

#### *Single cell separation*

Mice were anesthetized with pentobarbital sodium and transcardially perfused with 20 mL of sterile PBS to dissect the cortex. Cortical tissue was rinsed with Hanks' balanced salt solution (HBSS), mechanically dissociated, and enzymatically digested with papain using a Neural Tissue Dissociation Kit (P) (Miltenyl Biotec) in accordance with the instruction manual. For myelin removal, cells were resuspended in PBS with 0.9 M sucrose and centrifuged for 10 minutes at 400 g. The myelin-containing supernatant was removed, and the pelleted glial cells were washed with HBSS and processed for further analysis. To detect cytokine production in microglia, mice were intraperitoneally administered with 200  $\mu$ g of lipopolysaccharide (L8274, Sigma-Aldrich) 18 hours before the analysis. Prior to flow cytometric analysis, isolated glial cells were incubated for 4 hours with Dulbecco's modified Eagle's medium and Ham's F-12 nutrient mixture, 10% fetal bovine serum (FBS) and Golgi plug containing brefeldin A (BD). For the separation of neuronal cells, single cells separated from cortical tissue were treated with the Adult Mouse Neuron Isolation Kit (Miltenyl Biotec). Using a magnetic cell sorting system, negatively-selected neurons were collected.

#### *Flow cytometry*

Cells were treated with the Zombie Fixable Viability Kit (BioLegend) to discriminate between live and dead cells and then with anti-CD16/CD32 antibody (clone: 2.4G2) to block Fc receptors for 10 minutes before staining. Cell surface staining was performed using antibodies in PBS with 5% FBS and 5 mM ethylenediaminetetraacetic acid (EDTA). For intracellular staining, cells were fixed and permeabilized (Fixation/Permeabilization Solutions, BD) and then stained. Monoclonal antibodies for CD11b (clone: M1/70, BioLegend), CD45 (30-F11, BioLegend), CX3CR1 (SA011F11, BioLegend), CD140a (APA5, BioLegend), ACSA-2 (REA969, Miltenyl Biotec), MBP (2H9, Novus Biologicals), IL-12/IL-23p40 (C15.6, BioLegend), TUBB3 (TUJ1, BioLegend), phospho-Stat4 (4LURPIE, eBioscience) and phospho-Stat3 (13A3-1, BioLegend) were used. Stained cells were acquired on a CytoFLEX S (Beckman Coulter), and data were analyzed using FlowJo software (BD).



### *Golgi-Cox staining*

Golgi-Cox staining was performed using a superGolgi Kit (Bioenno Lifesciences) in accordance with the manufacturer's instructions. Brains were collected from mice after transcardial perfusion with 20 mL of cold normal saline. The dissected brain was cut into a block on the anterior side at approximately  $1 \times 2 \times 1 \text{ cm}^3$  to include the bilateral mPFC region. Stained brain blocks were cut into 200  $\mu\text{m}$  sections with a vibratome (Leica). The sections were mounted on gelatin-coated slides, stained, and then covered with Mount Quick (Daido Sangyo). Z-stacked images were acquired with the full focus function on a fluorescence microscope, BZ-X800 (Keyence, Japan).

### *Image quantification*

The images were analyzed using ImageJ software ver. 1.53c (National Institutes of Health, USA).

#### Neuronal activation analysis

Two immunofluorescent images of brain regions of interest (ROIs) with a  $20\times$  field for p-cFos staining were acquired per mouse. Activating neuronal cells were defined as p-cFos-positive DAPI-stained cells, and the number of cells were manually counted and then averaged to calculate the density per mouse.

#### Microglial activation state analysis

Two 50- $\mu\text{m}$  coronal sections containing the medial prefrontal cortex (mPFC) region were immunostained for Iba-1 and CD68. For each section, two  $20\times$  fields of full focused view were collected per mouse. The activation status of microglia was scored from 0 (lowest activation) to 4 (highest activation) depending on the CD68 expression pattern, which was analyzed and scored as 0-1 (no/scarce expression), 2 (punctate expression), 3 (multiple punctate expression), and 4 (aggregated expression). Activated microglia with an activation score of 3 or 4 were categorized as reactive microglia. The average percentage of reactive microglia was calculated for each mouse group.

#### Dendritic spine count

Four  $100\times$  coronal views of Golgi-Cox-stained sections containing mPFC layer 2/3 pyramidal neurons were obtained. For each view, 1-2 full focused neurons were included, and 5-7 dendrites from each neuron were recognized per mouse. The number of dendritic spines 40  $\mu\text{m}$  proximal to soma of impregnated pyramidal neurons in the mPFC, where the spine density is generally lower,<sup>2</sup> were counted per each dendrite. Since layer 2/3 pyramidal neurons are reported to be susceptible to chronic physiopsychological stress, we selected layer 2/3 pyramidal neurons for this analysis.

### *In vivo pharmacological intervention*

#### Osmotic pump intracerebroventricular administration of anti-IL-12/23p40 antibody

A monoclonal anti-IL-12/23p40 antibody (C17.8, BioLegend, 1 mg/mL diluted in saline) or mouse IgG2a isotype control antibody (MG2a-53, BioLegend, 1 mg/mL diluted in saline) was loaded into 200- $\mu\text{L}$  osmotic pumps (Alzet) with a 14-day infusion rate of 0.5  $\mu\text{L}$  per hour. Mice were implanted with osmotic pumps that were connected to a cannula (Brain Infusion Kit III, Alzet) inserted at +1.1 mm lateral, -0.5 mm anterior-posterior, and -2.5 mm deep from the bregma to target the right lateral ventricle. The pump was subcutaneously placed.

#### Systemic administration of Tyk2 inhibitor

Mice were intraperitoneally injected with 0.12 mg/kg of deucravacitinib diluted in dimethyl sulfoxide (10 mM, MedChemExpress, USA) or an equal volume of dimethyl sulfoxide daily for two weeks, followed by further analysis. The dosage of deucravacitinib was determined based on the clinical dose for psoriasis.

#### *Elevated plus maze test*

The maze consisted of two open and two closed arms that extended out from a central square. Each arm was 30 cm long and 5 cm wide. The platform was 50 cm above the floor. Mice were placed in the center area of the maze facing an open arm and allowed to explore the maze for 5 minutes. A video-tracking system Smart 3.0 (Panlab-Harvard Apparatus, USA) was used to record the time spent in open and closed arms. The proportion of the time spent in the open arm was used as a measure of anxiety-like behavior. The total distance mice travelled was a surrogate measurement of general locomotor activity.

#### *Open field test*

The open field chamber consisted of a square black base (50 cm × 50 cm) with opaque white walls 50 cm in height. Mice were allowed free exploration for 10 minutes and video-tracked. The proportion of time spent in the center zone was used to evaluate anxiety-like behavior. The total travelled distance was used as a measure of general locomotor activity.

#### *Brain stereotaxic microinjection*

An anesthetized 8-week-old MRL/MpJ control mouse was placed in a stereotaxic micromanipulator instrument (Narishige, Japan). Fur above the skull was shaved, and the skin was wiped with 70% ethanol. A 26s-gauge needle attached to a Hamilton syringe was pushed toward the mPFC region at +0.3 mm lateral, +1.8 mm anterior-posterior and -2.0 mm deep relative to the bregma. Recombinant mouse IL-12/23p40 (150 ng/0.5 µL, BioLegend) or PBS as vehicle were injected for over 8 minutes into the mPFC. After 48 hours, the mice were analyzed.

#### *Clinical data of patients with systemic lupus erythematosus (SLE)*

The patients included in this study met the 1997 update of the 1982 American College of Rheumatology (ACR) revised criteria or 2012 Systemic Lupus International Collaborating Clinics (SLICC) criteria for the classification of SLE.<sup>3,4</sup> Clinical data were extracted from medical records as follows: demographics such as sex, disease duration and disease activity index; complications including hypertension, diabetes mellitus and dyslipidemia; manifestations including non-neuropsychiatric symptoms such as skin rash, arthritis, nephritis and antiphospholipid syndrome as well as neuropsychiatric manifestations; laboratory findings such as anti-DNA antibody, anti-Ro/SSA antibody, antiphospholipid antibodies and complements; and treatments including glucocorticoids, immunosuppressants, and antithrombotic therapy. Disease activity was assessed by SLE disease activity index 2000 (SLEDAI-2K)<sup>5</sup> and SLICC/ACR damage index (SDI).<sup>6</sup> Patients with NPSLE were diagnosed based on clinical and laboratory assessments.<sup>7</sup> Diffuse manifestations in NPSLE are defined to include psychosis, acute confusional

state, mood disorder, and cognitive impairment, and focal manifestations are defined as neurological syndromes such as headache, seizure, cerebrovascular disease, demyelinating disease, and peripheral neuropathy. In this study, patients with meningitis and myelopathy were excluded to avoid too strong an effect on CSF cytokine levels by direct inflammation in the meninges and to evaluate inflammation inside the CNS.

#### *Human samples including serum and CSF*

We reviewed medical records to extract the clinical data of patients with SLE including NPSLE, whose serum and CSF were preserved at Hokkaido University (S-Table 1) or Kitasato University (S-Table 2) between 2006 and 2020. At the time of the new onset or relapse, serum and CSF samples were collected from the SLE patients. A lumbar puncture was performed with the patients in a lateral position, and the CSF was collected in polypropylene tubes. The samples were centrifuged at 1,000 g for 15 minutes at 4 °C, and the supernatants were aliquoted to avoid a freeze–thaw cycle and stored at –80 °C until further use. The serum and CSF samples of healthy controls were provided by the National Center of Neurology and Psychiatry Biobank, a member of the National Center Biobank Network (Tokyo, Japan). The CSF samples of patients with primary Sjögren’s syndrome (SS) were collected at Hokkaido University. Informed consent for the study was obtained from all patients included in this study or their relatives.

#### *Brain magnetic resonance imaging acquisition*

We obtained brain magnetic resonance (MR) images from 71 SLE patients at Hokkaido University Hospital from 2019 to 2020 (Table S3). All brain imaging data were obtained on a 3.0 T MRI scanner (Achieva TX, Philips Medical Systems) and a standard 32-channel radiofrequency head coil (Philips Medical Systems, Best, the Netherlands) at Hokkaido University Hospital. 3D-T1 magnetization-prepared rapid gradient echo (MPRAGE) images of the head were acquired with the following parameters: TR (repetition time) 6 ms, TE (echo time) 3 ms, flip angle 8°, field of view 24 cm × 24 cm, matrix size 240 × 240, slice thickness 1.0 mm, interslice gap 1.0 mm, and 180 sagittal slices. FLAIR (fluid-attenuated inversion recovery) image acquisition parameters were as follows: TR 10000 ms, TE 100 ms, TI (inversion time) 2700, ETL (echo train length) 20, field of view 20 cm × 20 cm, frequency encoding 256, phase encoding 192, slice thickness 5 mm, interslice gap 6.5 mm, and 23 axial slices.

#### *Voxel-based morphometric analysis*

MRI scans were processed by Brain Anatomical Analysis using Diffeomorphic deformation (BAAD) software (version 4.3, [www.shiga-med.ac.jp/~hqbioph/BAAD\(English\)/BAAD.html](http://www.shiga-med.ac.jp/~hqbioph/BAAD(English)/BAAD.html)). The brain was extracted from 3D-T1 MPRAGE images by a revised graph-cut-based skull-stripping, segmented into gray matter, white matter and CSF, and warped into Montreal Neurological Institute (MNI) space. Images were set around the anterior commissure-posterior commissure lines and re-sampled with a voxel size of 1 mm<sup>3</sup>. Tissue segmentation and bias correction of intensity non-uniformities were performed using an Adaptive Maximum A Posterior (AMAP) technique with Computational Anatomy Toolbox 12 (The Structural Brain Mapping Group at the University of Jena, Germany) to avoid a priori information on the tissue probabilities. Tissue Probability Maps were used for spatial normalization, initial skull-

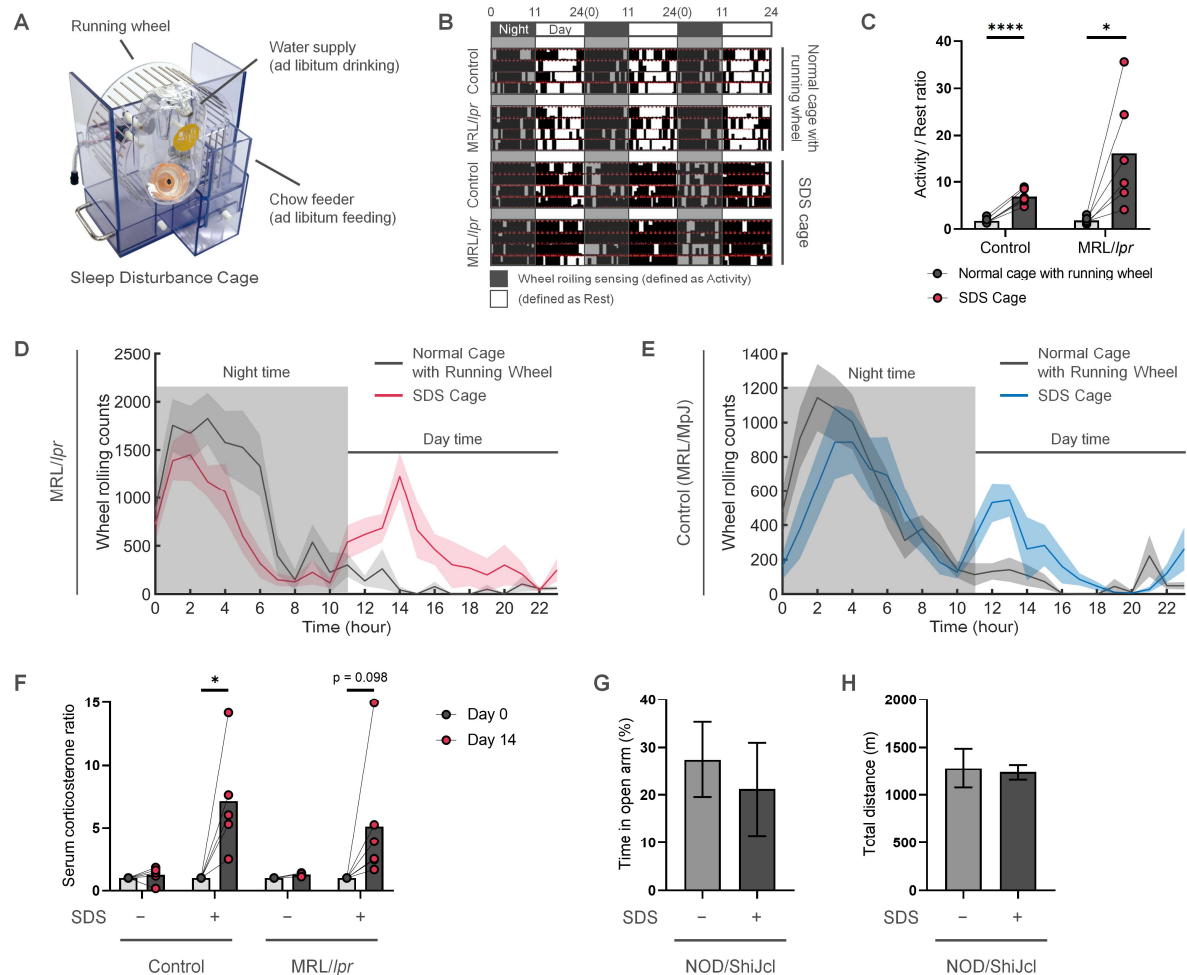
stripping and initial segmentation estimates. Before gray matter and white matter segmentation, an automated white matter lesion (WML) correction was conducted with the Lesion Segmentation Toolbox on FLAIR images by masking the averaged signal intensities of surrounding normal white matter. WML was divided into two regions, the periventricular area and deep white matter area, and both volumes were calculated using FLAIR images. For denoising, a spatial-adaptive Non-Local Means noise reduction filter and Markov Random Field approach were applied during AMAP segmentation. Coordinate transformation from native space to MNI space was conducted using the Diffeomorphic Anatomical Registration Through Exponentiated Lie Algebra (DARTEL) algorithm, resulting in voxel volume conversion into a voxel signal. ROI-wise volumetric analysis was performed with the MarsBar Toolbox (marsbar.sourceforge.net) using ROIs preset for the LONI Probabilistic Brain Atlas (LPBA40). An additional ROI of the bilateral mPFC was generated by combining brain masks of the Brainnetome Atlas (atlas.brainnetome.org). Local volume calculation was adjusted by total intracranial volume (TIV), age, sex and WML. For the Z-score estimation, age group-matched subjects in the Information eXtraction from Images (IXI) dataset were used as a reference, with age, sex, TIV and WM volume as confounding factors. Z-scores were calculated using the following equation.

$$Z \text{ score} = \frac{\text{Control mean} - \text{Individual value}}{\text{Control standard deviation}}$$

### Supplementary References

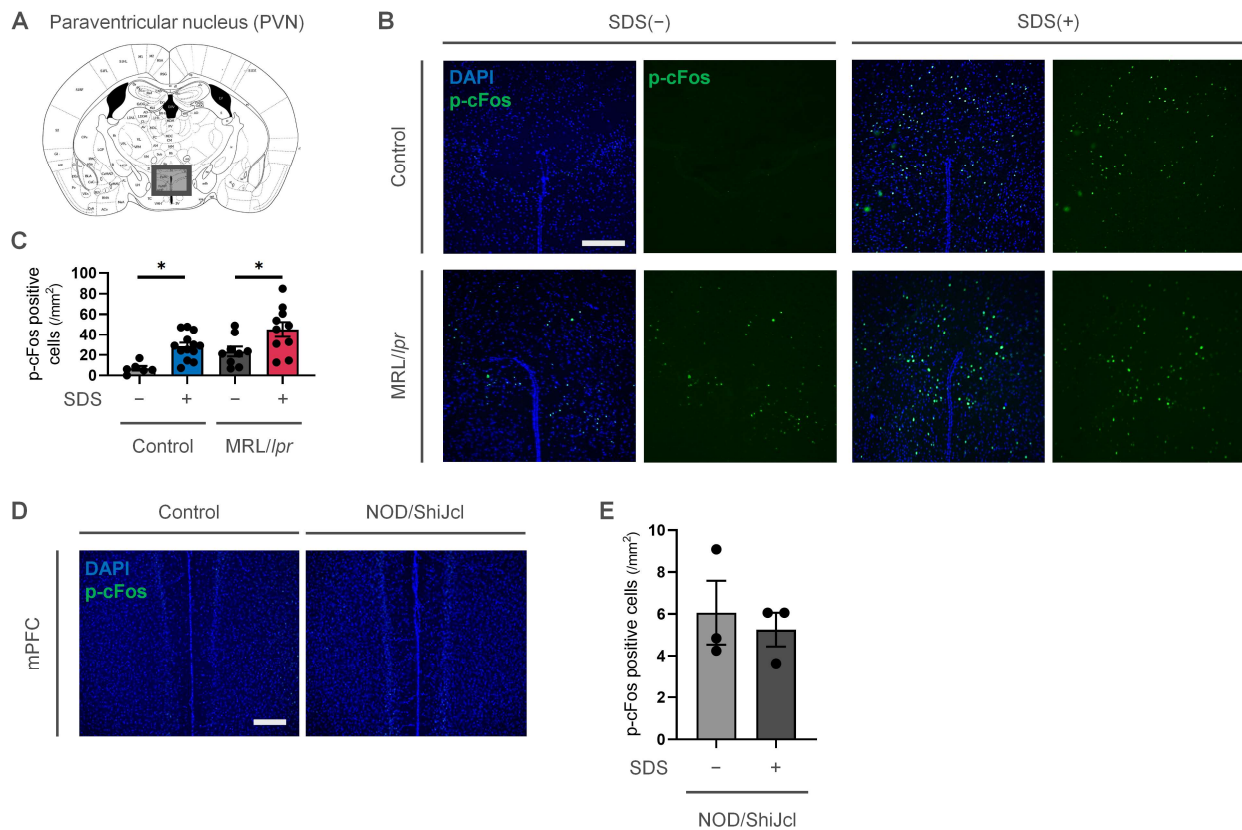
1. Jeltsch-David H, Muller S. Neuropsychiatric systemic lupus erythematosus and cognitive dysfunction: the MRL-lpr mouse strain as a model. *Autoimmun Rev* 2014;13:963-73.
2. Spruston N. Pyramidal neurons: dendritic structure and synaptic integration. *Nat Rev Neurosci* 2008;9:206-21.
3. Kaul A, Gordon C, Crow MK, et al. Systemic lupus erythematosus. *Nat Rev Dis Primers* 2016;2:16039.
4. Petri M, Orbai A-M, Alarcón GS, et al. Derivation and validation of the Systemic Lupus International Collaborating Clinics classification criteria for systemic lupus erythematosus. *Arthritis Rheum* 2012;64:2677-86.
5. Gladman DD, Ibañez D, Urowitz MB. Systemic lupus erythematosus disease activity index 2000. *J Rheumatol* 2002;29:288-91.
6. Gladman D, Ginzler E, Goldsmith C, et al. The development and initial validation of the Systemic Lupus International Collaborating Clinics/American College of Rheumatology damage index for systemic lupus erythematosus. *Arthritis Rheum* 1996;39:363-9.
7. Schwartz N, Stock AD, Putterman C. Neuropsychiatric lupus: new mechanistic insights and future treatment directions. *Nat Rev Rheumatol* 2019
8. Zhang Y, Chen K, Sloan SA, et al. An RNA-sequencing transcriptome and splicing database of glia, neurons, and vascular cells of the cerebral cortex. *J Neurosci* 2014;34:11929-47.

## Supplementary Figures



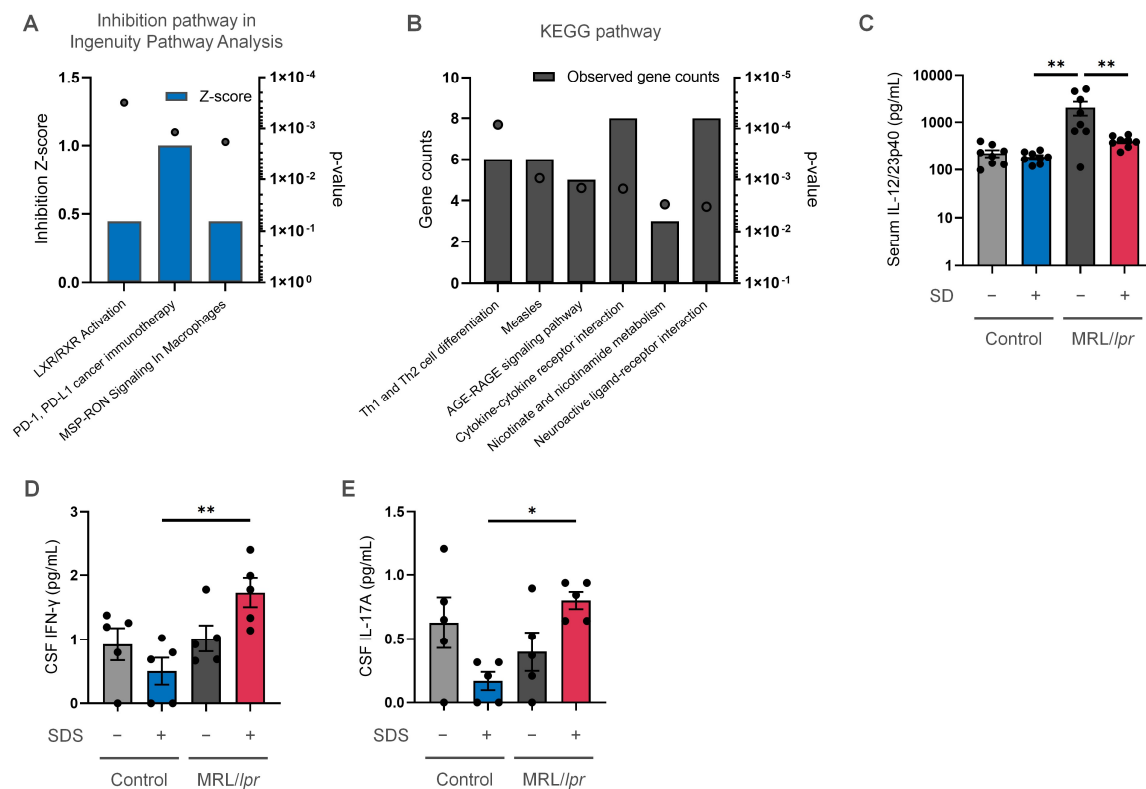
## Supplementary Figure 1. The effects of sleep disturbance stress (SDS).

(A) The appearance of the SDS cage equipped with a running wheel, water supply and chow feeder. (B) Representative images of the time-corresponding activity and rest in SDS-subjected, -free MRL/*lpr* and control mice. Black indicates wheel rolling sensation and is defined as activity; white indicates rest. SDS-subjected mice of both strains demonstrated more activity than SDS-free mice at night time. Each line corresponds to mouse activity for three days. (C) The activity (black) / rest (white) ratio ( $n = 6$  per group). (D, E) Descriptive images of wheel rolling counts to evaluate the circadian rhythm for daily activity in the presence or absence of SDS in (D) MRL/*lpr* and (E) control mice ( $n = 10$  to  $11$  per group). (F) Ratio of the serum corticosterone level in mice after 14 days of SDS relative to before SDS ( $n = 6$  per group). (G) Percentage of time spent in the open arms and (H) total travelled distance in SDS-subjected or -free NOD/ShiJcl mice ( $n = 5$  to  $7$  per group). (C, F) Data are means. \* $p < 0.05$ , \*\*\*\* $p < 0.0001$  using a paired t-test for paired data. (D, E) Data are means (line)  $\pm$  s.e.m. (band). (G, H) Data are means  $\pm$  s.e.m. An unpaired Student's t-test.



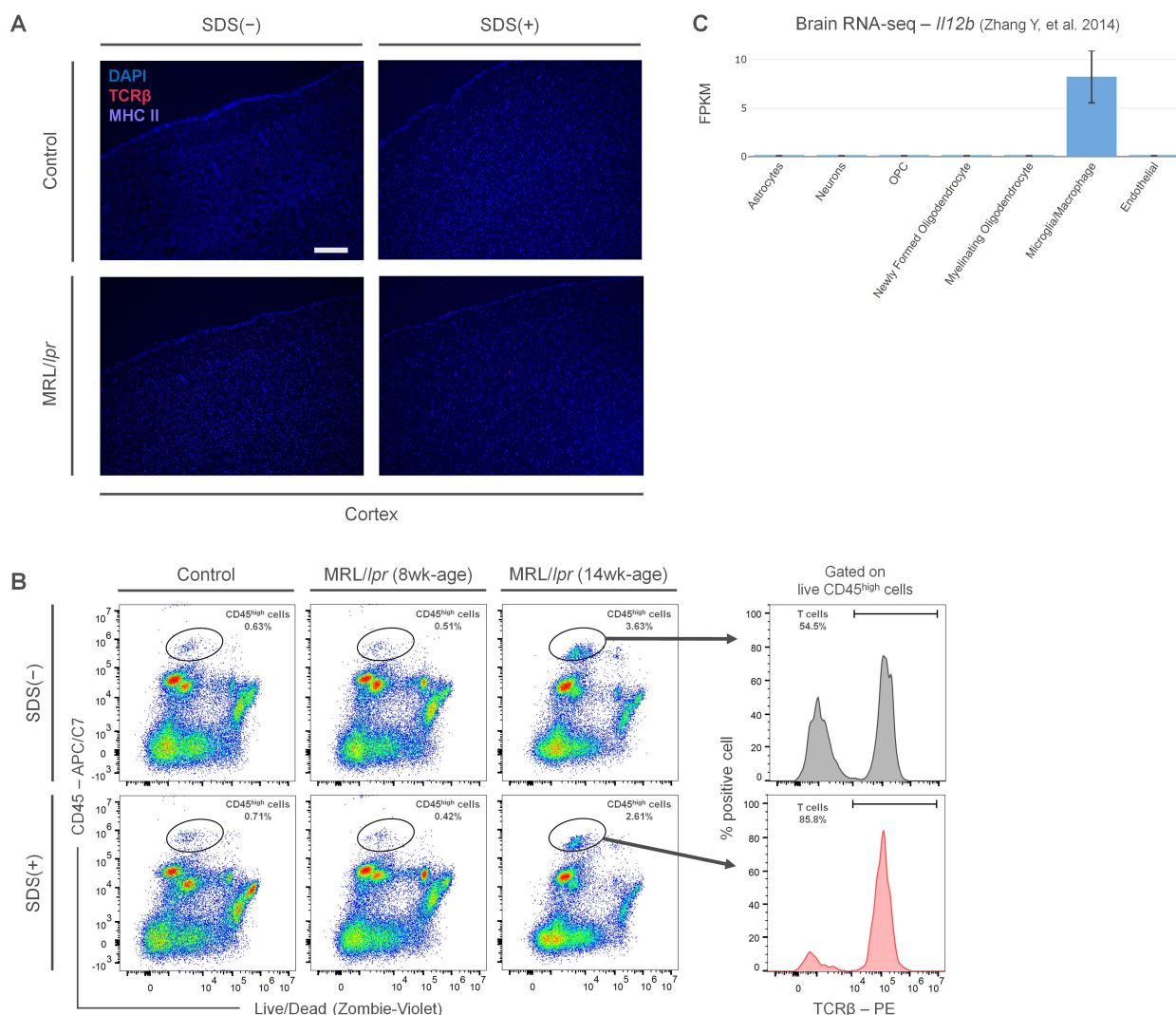
### Supplementary Figure 2. Neuronal activation of stress-responsive brain regions.

(A-E) Evaluation of neuronal activation using immunohistochemistry of phosphorylated cFos (p-cFos)-positive cells in the paraventricular nucleus (PVN) between sleep disturbance stress (SDS)-subjected or -free MRL/lpr, MRL/MpJ control, and NOD/ShiJcl mice. (A) Schematic drawing of the PVN was taken from Paxinos and Watson (2007). (B) Representative immunohistochemical images of neuronal activating p-cFos-positive cells with 4',6-diamidino-2-phenylindole (DAPI) in the PVN of MRL/lpr and MRL/MpJ control. Scale bar, 100  $\mu$ m. (C) Quantification of p-cFos-positive cells in the PVN ( $n = 6$  to 13 per group). (D) Representative immunohistochemical images of neuronal activating p-cFos-positive cells with DAPI in the mPFC of NOD/ShiJcl. Scale bar, 100  $\mu$ m. (E) Quantification of p-cFos-positive cells in the mPFC ( $n = 3$  per group). Data are means  $\pm$  s.e.m. \* $p < 0.05$  using a two-way ANOVA with the post-hoc Tukey-Kramer multiple comparison test or an unpaired Student's t-test.



### Supplementary Figure 3. Additional results of pathway analysis using public databases.

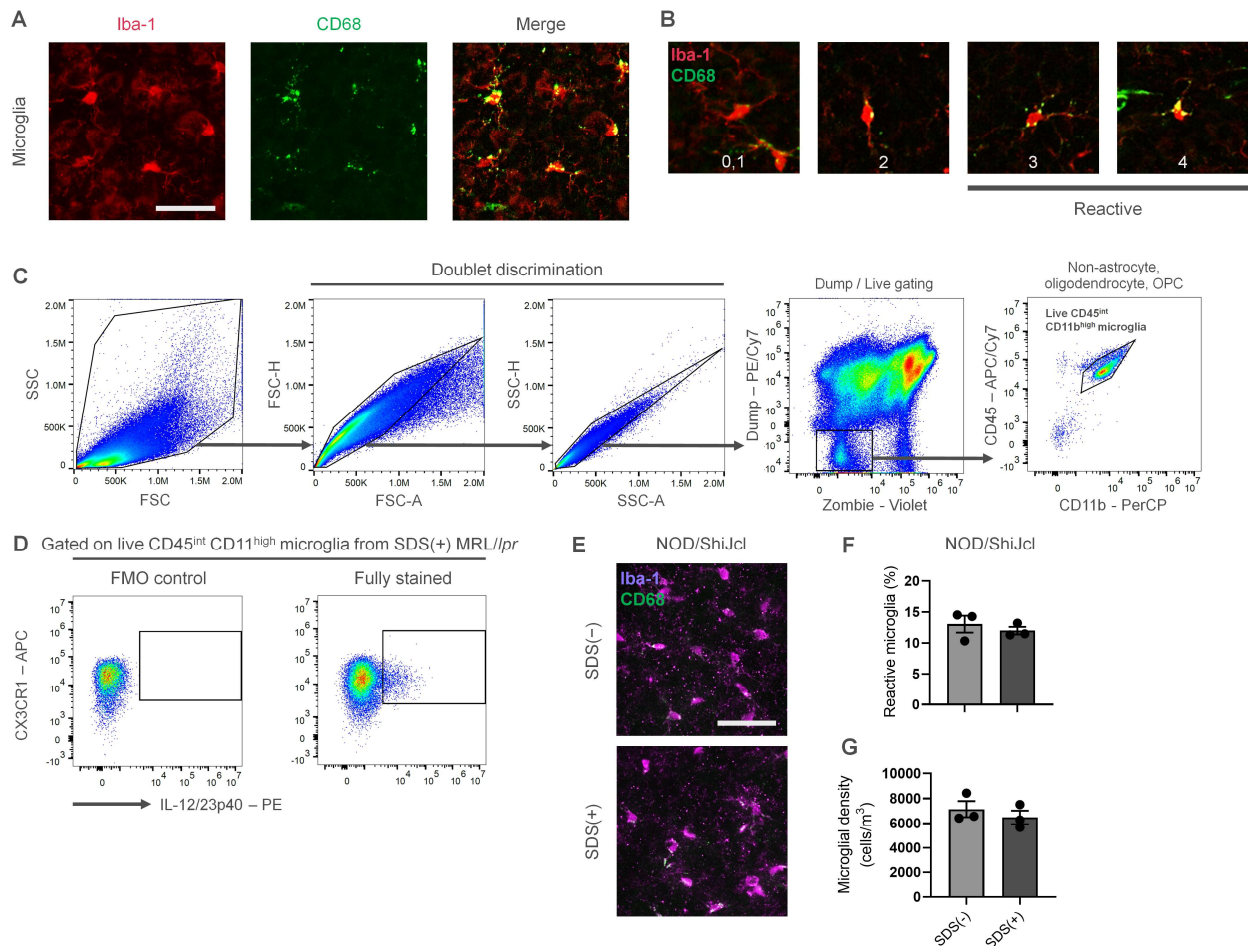
(A, B) (A) Ingenuity Pathway Analysis using the uniquely downregulated gene set and (B) KEGG (Kyoto Encyclopedia of Genes and Genomes) analysis using the uniquely upregulated and downregulated gene set in the prefrontal cortex of sleep disturbance stress (SDS)-subjected MRL/lpr mice. Bars show inhibition Z-scores or observed gene counts, and dots represent p-values. (C) Serum interleukin (IL)-12/23p40 levels measured by ELISA ( $n = 8$  per group). (D) CSF interferon (IFN)- $\gamma$  and (E) IL-17 A levels measured by multiplex beads assay ( $n = 5$  per group). Data are means  $\pm$  s.e.m. \* $p < 0.05$ , \*\* $p < 0.01$  using a two-way ANOVA with the Tukey-Kramer method.



**Supplementary Figure 4. Scarce infiltration of peripheral CD45<sup>high</sup> cells and specificity of *Il12b* expression in the CNS microglia/macrophages.**

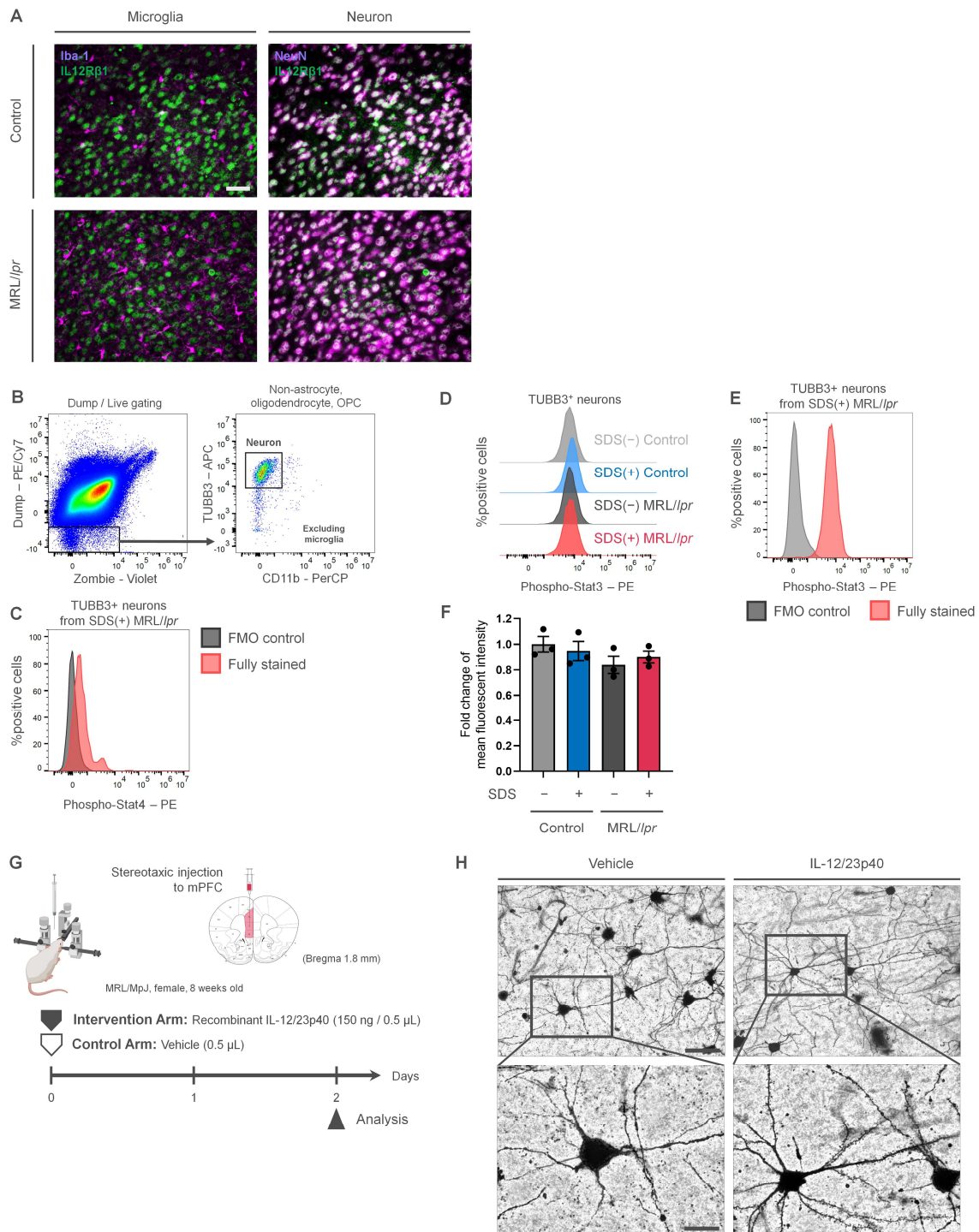
(A) Representative images of immunohistochemistry for TCRβ and/or MHC Class II (I-A/I-E)-positive cells in the cerebral cortex of SDS-subjected, -free MRL/lpr, and control mice. Scale bar, 100 μm. (B) Representative gating images for the isolated cortex to evaluate CD45<sup>high</sup> cell infiltration. CD45<sup>high</sup> cells, especially with TCRβ positivity, infiltrated the CNS of MRL/lpr mice in an age-dependent manner independently of the SDS load, confirming the scarce CNS infiltration of CD45<sup>high</sup> cells in 6-to-8-week-old MRL/lpr mice. (C) *Il12b* gene expression in mouse CNS cells shows prominent expression in microglia and macrophages. RNA-seq data from the Barres lab ([www.brainrnaseq.org/](http://www.brainrnaseq.org/)).<sup>8</sup> Data are means ± s.e.m.





### Supplementary Figure 5. Activation state analysis and gating strategy in microglia.

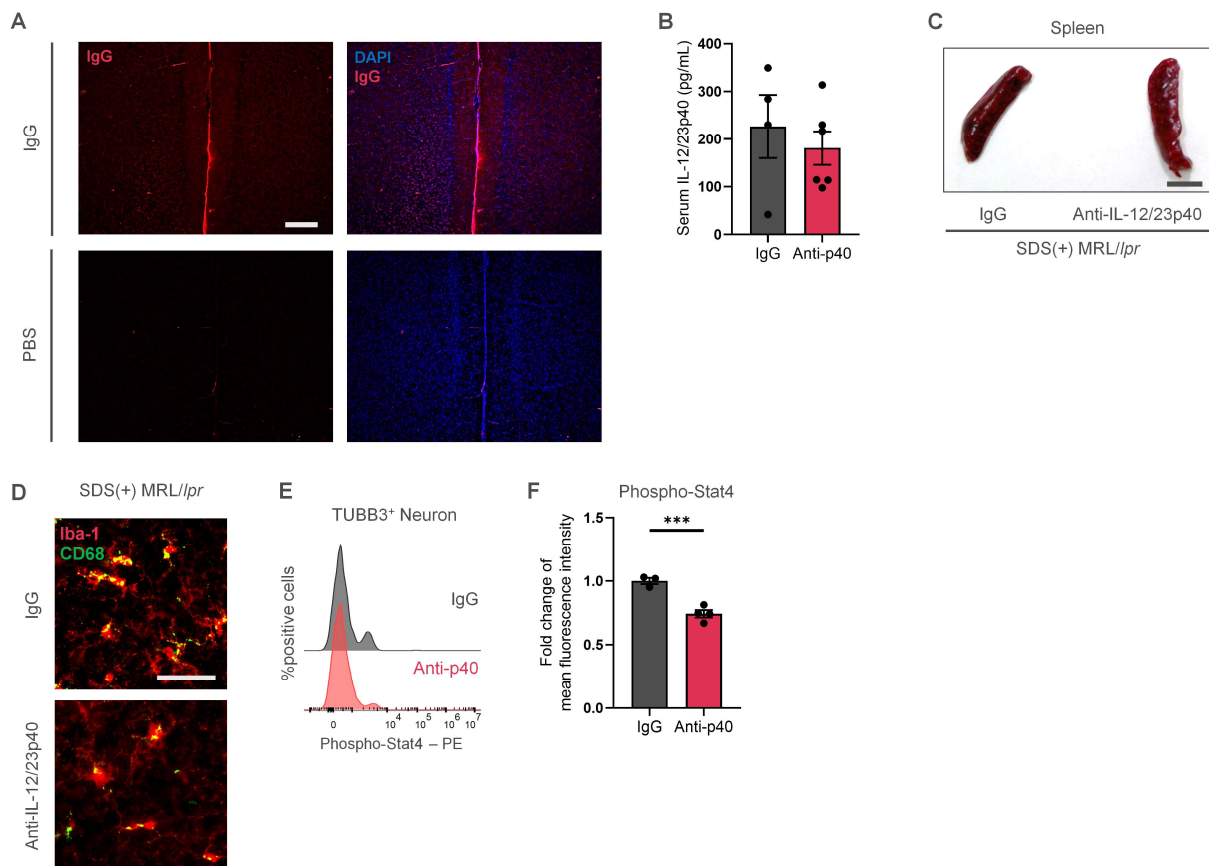
(A) Representative images of Iba-1 and CD68 staining. Scale bar, 50  $\mu\text{m}$ . (B) Microglial activation state scores in microglial activation analysis. Microglia falling into the category of 3 or higher were defined as reactive microglia. (C) Representative images of the gating strategy for identifying microglia. After doublet discrimination, Zombie-positive (dead) cells and dump cells including ACSA-2 (astrocyte), CD140a (oligodendrocyte precursor cell) and MBP (myelin basic protein: oligodendrocyte) positive cells were excluded. Gated  $\text{CD45}^{\text{int}}\text{CD11b}^{\text{high}}$  cells were selected as live microglia. (D) Flow cytometric gating of (right) fluorescence minus one (FMO) negative control and (left) fully stained samples from SDS-subjected MRL/lpr mice. (E) Representative images of mPFC microglia of the NOD/ShiJcl. (F) Percentage of reactive microglia and (G) microglial density of the NOD/ShiJcl ( $n = 3$  per group). Data are means  $\pm$  s.e.m. An unpaired Student's t-test.



### Supplementary Figure 6. Neuronal expression analysis and stereotaxic microinjection with IL-12/23p40.

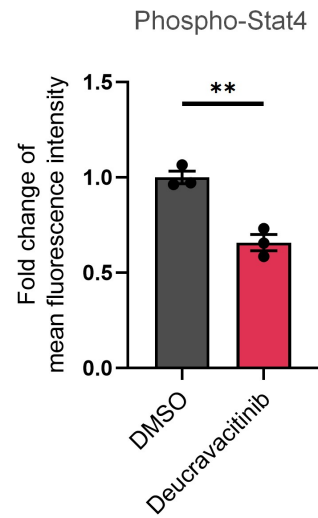
(A) Co-expression analysis of IL12R $\beta$ 1 by immunohistochemistry for microglia as Iba-1-positive cells and neurons as NeuN-positive cells. Scale bar, 50  $\mu$ m. (B) Representative images of the gating strategy to identify neurons. After doublet discrimination, Zombie-positive (dead) cells and dump cells including astrocytes,

microglia, oligodendrocytes and oligodendrocyte precursor cells were excluded. Gated TUBB3<sup>+</sup> cells were selected as live neurons. **(C)** Flow cytometric histogram of (gray) FMO negative controls and (red) fully stained samples from SDS-subjected MRL/*lpr* mice. **(D)** Representative histogram for phosphorylated-Stat3 in the mPFC neurons. **(E)** Flow cytometric histogram of FMO negative controls and fully stained samples from SDS-subjected MRL/*lpr* mice. **(F)** Fold-change of the mean fluorescence intensity for the phosphorylated-Stat3 expression relative to SDS-free control mice ( $n = 3$  per group). Data are means  $\pm$  s.e.m. A two-way ANOVA with the Tukey-Kramer method. **(G)** Experimental design for the evaluation of the IL-12/23p40 effect on mPFC neuronal cells by the stereotaxic microinjection model. **(H)** Golgi-Cox staining of neurons in the mPFC of IL-12/23p40-injected or vehicle-injected MRL/MpJ mice. Lower panels are magnified images of the rectangular areas in the upper panels. Scale bars, (upper panel) 50  $\mu$ m, and (lower panel) 20  $\mu$ m.



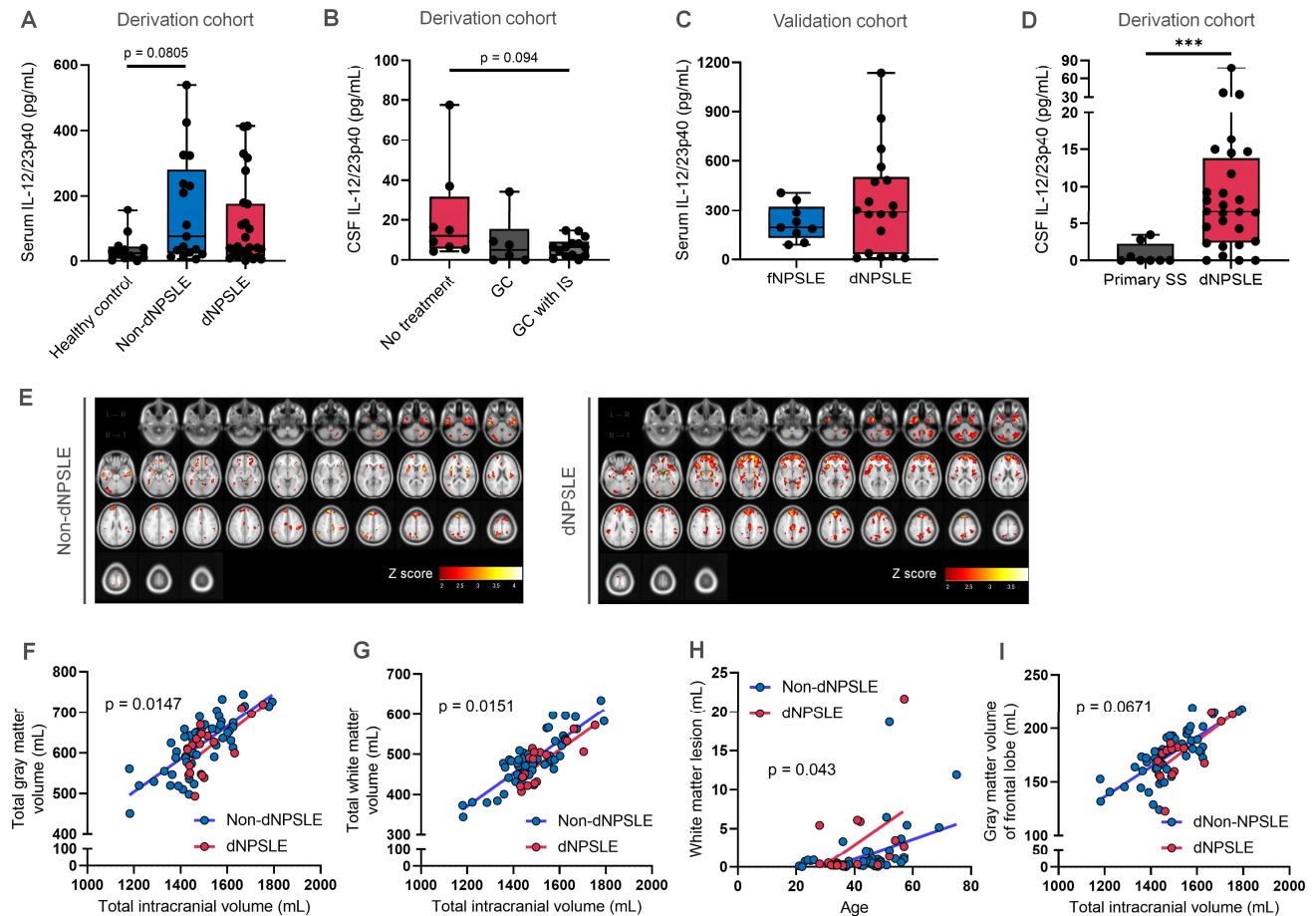
### Supplementary Figure 7. The effects of IL-12/23 signaling blockade therapy in the CNS of stress-subjected MRL/lpr mice.

(A) Representative images of the mPFC in IgG-treated or PBS-treated mice with osmotic pumps indicate successful antibody distribution throughout the mPFC. (B) No effect of anti-IL-12/23p40 blockade in the CNS on the serum IL-12/23p40 level was detected by ELISA ( $n = 4$  to 6 per group). (C) Macroscopic findings of the spleen in anti-p40 antibody- or IgG-treated SDS-subjected MRL/lpr mice. (D) Representative images of activated microglia. (E) Representative histogram of the phosphorylated-Stat4 expression in TUBB3<sup>+</sup> neurons. (F) Fold-change in the mean fluorescence intensity of the phosphorylated-Stat4 expression in TUBB3<sup>+</sup> neurons relative to controls ( $n = 3$  per group). Scale bars, (A) 100  $\mu$ m, (C) 10 mm, and (D) 50  $\mu$ m. Data are means  $\pm$  s.e.m. \*\*\* $p < 0.001$  using an unpaired Student's *t*-test.



**Supplementary Figure 8. Additional information for the results of experiments using Tyk2 inhibitor.**

Fold-change in the mean fluorescence intensity of phosphorylated-Stat4 expression in TUBB3+ neurons of deucravacitinib-treated SDS-subjected MRL/*lpr* mice relative to vehicle-treated mice ( $n = 3$  per group). Data are means  $\pm$  s.e.m. \*\* $p < 0.01$  using an unpaired Student's t-test.



### Supplementary Figure 9. Specificity of CSF IL-12/23p40 and brain atrophy in NPSLE patients with diffuse manifestations (dNPSLE).

(A) Serum IL-12/23p40 levels in the derivation cohort at Hokkaido University Hospital ( $n = 12$  healthy controls,  $n = 17$  non-dNPSLE,  $n = 26$  dNPSLE). (B) CSF IL-12/23p40 levels in dNPSLE patients ( $n = 8$  no treatment,  $n = 6$  glucocorticoid (GC),  $n = 14$  GC combined with immunosuppressants (IS)). (C) Serum IL-12/23p40 levels in the validation cohort at Kitasato University Hospital ( $n = 9$  NPSLE with focal manifestations (fNPSLE),  $n = 18$  dNPSLE). (D) CSF IL-12/23p40 levels at Hokkaido University Hospital ( $n = 8$  primary Sjögren's syndrome (SS),  $n = 26$  dNPSLE). (E) Representative serial axial brain images on which the Z-scores of brain atrophy were rendered in a non-dNPSLE and a dNPSLE patient. (F-I) Voxel-based morphometric analysis of patients with non-dNPSLE (blue,  $n = 56$ ) and dNPSLE (red,  $n = 15$ ) to compare (F) total gray matter volume, (G) total white matter volume (WMV) corresponding to total intracranial volume (TIV), (H) WM lesions volume corresponding to age, and (I) the bilateral frontal cortex volume corresponding to TIV. (A-E) Data are medians (interquartile range). Statistical analysis was performed using a Kruskal-Wallis test with post-hoc Steel-Dwass method or a Mann-Whitney U test. (F-I) ANCOVA adjusting for age, sex, disease duration of SLE and TIV.

## Supplementary Tables

**Supplementary Table 1. Demographic and clinical characteristics of SLE patients at Hokkaido University Hospital for IL-12/23p40 measurements.**

Characteristics	All SLE (n=47)	Non-dNPSLE (n=19)	dNPSLE (n=28)
<b>Demographics</b>			
Age at lumbar puncture, years	30 [23-41]	29 [21-37]	31 [25-44]
Sex, female	40 (85%)	18 (95%)	22 (79%)
Disease duration, years	6 [0-15]	2 [0-9]	11 [0-17]
SLEDAI-2K	14 [10-19]	12 [8-16]	15 [11-22]
<b>Disease classification at the time of sampling</b>			
New onset	18 (38%)	12 (63%)	6 (21%)
Relapse	29 (62%)	7 (37%)	22 (89%)
<b>Complications</b>			
Hypertension	13 (28%)	4 (21%)	9 (32%)
Dyslipidemia	7 (15%)	2 (11%)	5 (18%)
Diabetes	2 (4%)	0	2 (7%)
<b>Symptoms except diffuse neuropsychiatric manifestations</b>			
Rash	16 (34%)	8 (42%)	8 (29%)
Oral ulcer	7 (15%)	4 (21%)	3 (11%)
Arthritis	11 (23%)	6 (32%)	5 (18%)
Myositis	1 (2%)	1 (5%)	0
Serositis	5 (11%)	4 (21%)	1 (4%)
Nephritis	12 (26%)	7 (37%)	5 (18%)
Headache	1 (2%)	1 (5%)	0
Peripheral neuropathy	2 (4%)	2 (11%)	0
Seizure	0		
Leucopenia	14 (30%)	8 (42%)	6 (21%)
Hemolytic anemia	6 (13%)	3 (16%)	3 (11%)
Thrombocytopenia	11 (23%)	7 (37%)	4 (14%)
Hemophagocytic syndrome	2 (4%)	2 (11%)	0
Antiphospholipid syndrome	3 (6%)	1 (5%)	2 (7%)
<b>Classification of diffuse neuropsychiatric manifestations</b>			
Anxiety			0
Mood disorder			8 (29%)
Cognitive dysfunction			1 (6%)
Psychosis			4 (14%)
Acute confusional state			15 (54%)
<b>Laboratory findings</b>			
<i>Serum</i>			

Immunoglobulin G (IgG), mg/dL	1599 [983-2016]	1599 [981-2212]	1609 [998-1912]
Anti-DNA antibody (RIA), IU/mL	9.8 [0-170.2]	21 [0-278.1]	9.8 [0-42.3]
Anti-dsDNA antibody (ELISA), IU/mL	8 [0-92.1]	26.4 [0-93.3]	0 [0-147.7]
Anti-Ro/SSA antibody, U/mL	39.7 [0-126.9]	59.4 [10.2-136.5]	29.9 [0-117.5]
Anti-cardiolipin (CL) IgG	10/16 (62%)	3/5 (60%)	7/11 (64%)
Anti-CL/ $\beta$ 2-glycoprotein complex antibody	5 (11%)	2 (13%)	3 (11%)
Lupus anticoagulant (DRVVT)	13 (37%)	6 (46%)	7 (32%)
Complement C3, mg/dL	57 [32-87]	47 [30-107]	70 [40-82]
Complement C4, mg/dL	10 [3-17]	6 [3-27]	11 [2.3-16]
CH50, IU/mL	26.1 [10.1-48.1]	16.4 [9.6-55.7]	29.8 [10.9-45.8]
<i>Cerebrospinal fluid</i>			
cell count, / $\mu$ L	1 [0-3]	1 [0-3]	1 [0-3]
mononuclear cell count, / $\mu$ L	1 [0-3]	1 [0-3]	1 [0-2.8]
Protein, mg/dL	30 [23-46]	26 [21.8-41.5]	35.5 [23.8-55.8]
Glucose, mg/dL	55 [52-68]	55 [53-66.8]	54 [50.3-70.3]
IgG index, ratio	0.82 [0.73-0.97]	0.76 [0.68-0.93]	0.85 [0.73-0.98]
Interleukin-6 (IL-6), pg/mL	5.9 [2.5-15.5]	2.9 [1.9-5.6]	8.9 [3.2-26.3]
IL-8, pg/mL	48.9 [4.98-160.8]	23.5 [1-45.9]	99.9 [17.7-186.3]
<b>Treatment</b>			
Glucocorticoid	33 (70%)	12 (63%)	21 (75%)
- glucocorticoid dose at CSF collection		30 [14-40]	20 [10-56]
Cyclophosphamide	6 (13%)	2 (11%)	4 (14%)
Mycophenolate mofetil	4 (9%)	2 (11%)	2 (7%)
Azathioprine	3 (6%)	0	3 (11%)
Hydroxychloroquine	2 (4%)	0	2 (7%)
Tacrolimus	7 (15%)	5 (26%)	2 (7%)
Cyclosporine	4 (9%)	0	4 (14%)
Belimumab	1 (2%)	1 (5%)	0
Warfarin	1 (2%)	1 (5%)	0
Direct oral anticoagulant	0	0	0
Aspirin	7 (15%)	3 (16%)	4 (14%)
Clopidogrel	1 (2%)	0	1 (4%)
Cilostazol	3 (6%)	2 (11%)	1 (4%)
Sleep medication	26 (55%)	6 (32%)	20 (71%)

Values are presented as n (%) or medians (interquartile range).

Abbreviations: SLE, systemic lupus erythematosus; NP, neuropsychiatric; dNPSLE, NPSLE with diffuse manifestations; SLEDAI-2K, Systemic Lupus Erythematosus Disease Activity Index 2000; DRVVT, dilute Russel's viper venom time; CH50, 50% hemolytic complement activity



**Supplementary Table 2. Demographic and clinical characteristics of NPSLE patients at Kitasato University Hospital for IL-12/23p40 measurements.**

Characteristics	All NPSLE (n=27)	fNPSLE (n=9)	dNPSLE (n=18)
<b>Demographics</b>			
SLEDAI-2K	13 [10-18]	6 [0-16]	15 [12-19]
<b>Disease onset</b>			
Initial onset	12 (44%)	3 (33%)	9 (50%)
Relapse	15 (56%)	6 (67%)	9 (50%)
<b>Complications</b>			
Hypertension	3 (11%)	0	3 (17%)
Dyslipidemia	0		
Diabetes	2 (7%)	0	2 (11%)
<b>Symptoms except diffuse neuropsychiatric manifestations</b>			
Rash	7 (26%)	0	7 (39%)
Oral ulcer	3 (11%)	1 (11%)	2 (11%)
Arthritis	4 (15%)	1 (11%)	3 (17%)
Myositis	1 (2%)	0	1 (6%)
Serositis	5 (19%)	0	5 (28%)
Nephritis	10 (37%)	2 (22%)	8 (44%)
Headache	1 (2%)	1 (11%)	0
Peripheral neuropathy	6 (22%)	6 (67%)	0
Seizure	2 (7%)	2 (22%)	0
Leucopenia	2 (7%)	2 (22%)	1 (6%)
Hemolytic anemia	2 (7%)	0	2 (11%)
Thrombocytopenia	3 (11%)	0	3 (17%)
Hemophagocytic syndrome	2 (7%)	1 (11%)	1 (6%)
Antiphospholipid syndrome	10 (37%)	4 (44%)	6 (33%)
<b>Classification of diffuse neuropsychiatric manifestations</b>			
Anxiety			1 (6%)
Mood disorder			2 (11%)
Cognitive dysfunction			0
Psychosis			3 (17%)
Acute confusional state			12 (67%)
<b>Laboratory findings</b>			
<i>Serum</i>			
Immunoglobulin G (IgG), mg/dL	1654 [1159-2004]	1691 [1270-2915]	1602 [1120-1891]
Anti-DNA antibody (RIA), IU/mL	8.9 [0-44]	3.8 [0-32]	9.4 [3.93-76.8]
Anti-dsDNA antibody (ELISA), IU/mL	8 [0-92.1]	23 [23-23]	23 [10-56]
Anti-Ro/SSA antibody	16 (59%)	6 (67%)	10 (56%)

Anti-NR2 antibody	8 (33%)	4 (50%)	4 (25%)
Anti-cardiolipin (CL) IgG	9 (33%)	4 (44%)	5 (28%)
Anti-CL/ $\beta$ 2-glycoprotein complex antibody	4 (15%)	2 (22%)	2 (11%)
Lupus anticoagulant (DRVVT)	6 (22%)	2 (22%)	4 (22%)
Complement C3, mg/dL	65 [40-79]	78 [59.5-127]	58 [37-76.8]
Complement C4, mg/dL	17 [5-23]	18 [9-36]	13 [5-20]
CH50, IU/mL	31 [12-40]	40 [20.5-49.5]	27.5 [11.5-36]
<i>Cerebrospinal fluid</i>			
cell count, / $\mu$ L	2 [0-12]	3 [0-23]	2 [0-13]
mononuclear cell count, / $\mu$ L	2 [0-7]	3 [0-23]	2 [0-9]
Protein, mg/dL	64 [37-104]	46 [34.5-74]	83.5 [48.3-124]
Glucose, mg/dL	58 [46-72]	59 [47-71]	54 [46-74]
IgG index, ratio	0.56 [0.49-0.74]	0.53 [0.44-0.69]	0.60 [0.49-0.76]
Interleukin-6 (IL-6), pg/mL	18.5 [4.1-150.8]	30.7 [2.2-941]	15.1 [4.85-110.1]
Anti-NR2 antibody	17 (74%)	6 (86%)	11 (69%)
<b>Treatment</b>			
Glucocorticoid	27 (100%)	9 (100%)	18 (100%)
Cyclophosphamide	10 (37%)	2 (22%)	8 (44%)
Mycophenolate mofetil	2 (7%)	0	2 (11%)
Azathioprine	1 (4%)	0	1 (6%)
Hydroxychloroquine	3 (11%)	1 (11%)	2 (11%)
Tacrolimus	4 (15%)	0	3 (17%)
Cyclosporine	4 (9%)	1 (11%)	3 (17%)
Belimumab	1 (4%)	0	1 (6%)
Warfarin	5 (19%)	1 (11%)	4 (22%)
Direct oral anticoagulant	0	0	0
Aspirin	6 (22%)	3 (33%)	3 (17%)
Clopidogrel	1 (4%)	0	1 (6%)
Cilostazol	1 (4%)	0	1 (6%)

Values are presented as n (%) or medians (interquartile range).

Abbreviations: NPSLE, neuropsychiatric systemic lupus erythematosus; fNPSLE, NPSLE with focal manifestations; dNPSLE, NPSLE with diffuse manifestations; SLEDAI-2K, Systemic Lupus Erythematosus Disease Activity Index 2000; NR2, N-Methyl-D-Aspartic Acid Receptor 2; DRVVT, dilute Russel's viper venom time; CH50, 50% hemolytic complement activity

**Supplementary Table 3. Demographic and clinical characteristics of SLE patients at Hokkaido University Hospital used in VBM analysis.**

Characteristics	All SLE (n=71)	Non-dNPSLE (n=56)	dNPSLE (n=15)
<b>Demographics</b>			
Age at image acquisition, years	43 [36-49]	45 [37-49]	41 [31-52]
Sex, female	65 (92%)	53 (95%)	12 (80%)
Disease duration, years	11 [7-19]	11 [6-18]	16 [7-21]
SLICC Damage index	1 [0-1]	0.5 [0-1]	1 [1-2]
<b>Complications</b>			
Hypertension	24 (34%)	18 (32%)	6 (40%)
Dyslipidemia	28 (39%)	20 (36%)	8 (53%)
Diabetes	2 (3%)	2 (4%)	0
<b>Disease classification</b>			
NPSLE	17 (24%)	2 (11%)	15 (100%)
- Focal manifestations (fNPSLE)	- 2 (12%)	- 2 (100%)	- 0
- Diffuse manifestations (dNPSLE)	- 15 (88%)	- 0	- 15 (100%)
Antiphospholipid syndrome	38 (54%)	30 (54%)	8 (53%)
<b>Voxel based morphometric parameters</b>			
Stroke or white matter lesions	35 (49%)	24 (43%)	11 (73%)
Total intracranial volume, mL	1469 [1430-1571]	1466 [1418-1570]	1482 [1440-1632]
Cerebrospinal fluid, mL	380 [345-435]	366 [340-424]	445 [380-501]
<b>Laboratory findings</b>			
<i>Serum</i>			
Antinuclear antibody	67 (94%)	53 (95%)	14 (93%)
Anti-DNA antibody (RIA), IU/mL	2.75 [0.35-11.4]	3.9 [0-19.3]	2.5 [1-4.5]
Anti-dsDNA antibody (ELISA), IU/mL	0.6 [0-14.7]	0.6 [0-18.7]	0.7 [0-5.8]
Anti-Ro/SSA antibody	19.6 [0-122]	11.5 [0-121]	56 [1.4-138]
Anti-cardiolipin (CL) IgG	12/24 (50%)	10/19 (53%)	2/5 (40%)
Anti-CL/β2-glycoprotein complex antibody	23 (41%)	18 (32%)	5 (33%)
Lupus anticoagulant (DRVVT)	27 (38%)	20 (36%)	7 (47%)
Complement C3, mg/dL	91 [72-112]	90 [72.3-112]	99 [65-112]
Complement C4, mg/dL	19 [11-24]	18 [11-24]	20 [12-27]
CH50, IU/mL	48.8 [37.3-54.6]	49.1 [37.2-55.9]	46.8 [38.5-54.1]
<b>Treatment</b>			
Glucocorticoid	58 (82%)	43 (77%)	15 (100%)
Mycophenolate mofetil	13 (18%)	8 (14%)	5 (33%)
Azathioprine	5 (7%)	4 (7%)	1 (7%)
Hydroxychloroquine	23 (32%)	18 (32%)	5 (33%)
Tacrolimus	29 (41%)	21 (38%)	8 (53%)

Belimumab	2 (3%)	1 (2%)	1 (7%)
Sleep medication	15 (21%)	10 (18%)	5 (33%)
Post-treatment history of cyclophosphamide	17 (24%)	7 (13%)	10 (67%)
Anticoagulation	14 (20%)	10 (18%)	4 (27%)
- Warfarin	- 11 (79%)	- 9 (90%)	- 2 (50%)
- Direct oral anticoagulant	- 3 (21%)	- 1 (18%)	- 2 (50%)
Antiplatelets	31 (44%)	25 (44%)	6 (40%)
- Aspirin	- 25 (81%)	- 20 (80%)	- 5 (83%)
- Clopidogrel	- 11 (35%)	- 9 (38%)	- 2 (33%)
- Cilostazol	- 2 (7%)	- 2 (8%)	- 0

Values are presented as n (%) or medians (interquartile range).

Abbreviations: NPSLE, neuropsychiatric systemic lupus erythematosus; dNPSLE, NPSLE with diffuse manifestations; fNPSLE, NPSLE with focal manifestations; SLICC, Systemic Lupus International Collaborating Clinics; DRVVT, dilute Russel's viper venom time; CH50, 50% hemolytic complement activity

**Supplementary Table 4. Sleep medications prescribed to the SLE patients in the Hokkaido University Hospital cohort**

Characteristics	All SLE ( <i>n</i> =26)	Non-dNPSLE ( <i>n</i> =6)	dNPSLE ( <i>n</i> =20)
<b>Benzodiazepines</b>			
Brotizolam	12 (46%)	4 (67%)	8 (40%)
Clonazepam	2 (8%)	1 (17%)	1 (5%)
Flunitrazepam	3 (12%)	0	3 (15%)
Etizolam	2 (8%)	0	2 (10%)
Lormetazepam	2 (8%)	0	2 (10%)
Lorazepam	3 (12%)	0	3 (15%)
<b>Imidazopyridine</b>			
Zolpidem	4 (15%)	1 (17%)	3 (15%)
<b>Cyclopyrrolone</b>			
Zopiclone	1 (4%)	0	1 (5%)
<b>Melatonin receptor agonist</b>			
Ramelteon	1 (4%)	0	1 (5%)

Values are presented as *n* (%).